MOLECULAR DYNAMICS SIMULATION OF THE THERMAL PROPERTIES OF Y-JUNCTION CARBON NANOTUBES

By

ARON WILLIAM CUMMINGS

A thesis submitted in partial fulfillment of
the requirements for the degree of

MASTER OF SCIENCE IN ELECTRICAL ENGINEERING

WASHINGTON STATE UNIVERSITY
Department of Electrical Engineering and Computer Science

August 2004

To the Faculty of Washington State University:

The members of the Committee appointed to examine the thesis of ARON WILLIAM CUMMINGS find it satisfactory and recommend that it be accepted.

_____
Chair

_____

_____

ACKNOWLEDGEMENTS

Aron Cummings would like to acknowledge the financial support of a graduate fellowship from Washington State University's school of Electrical Engineering and Computer Science, and of the Department of Energy's Computational Science Graduate Fellowship provided under grant number DE-FG02-97ER25308. He would also like to acknowledge support provided by Deepak Srivastava through a NASA Ames Education Associates summer internship at NASA's Ames Research Center. He would like to thank his committee members, Dr. Pedrow and Dr. McCluskey, for their input. Finally, he would like to acknowledge the significant counsel provided by his advisor, Dr. Mohamed Osman.

MOLECULAR DYNAMICS SIMULATION OF THE THERMAL

PROPERTIES OF Y-JUNCTION CARBON NANOTUBES

Abstract

by Aron William Cummings, M.S.
Washington State University
August 2004

Chair: Mohamed A. Osman

Molecular dynamics simulations have been used to investigate the thermal properties of a Y-junction carbon nanotube consisting of a (14,0) trunk splitting into a pair of (7,0) branches. Steady state simulations were used to calculate the thermal conductivity of the Y-junction nanotube over a range of temperatures. It was found that the thermal conductivity of the Y-junction nanotube is less than that of a corresponding straight (14,0) nanotube, due to lattice defects in the form of non-hexagonal carbon rings at the junction. These lattice defects result in a discontinuity in the temperature profile of the Y-junction nanotube. Defects that were introduced to a straight (14,0) nanotube resulted in a similar discontinuity in the temperature profile. Phonon spectra revealed that the presence of lattice defects suppresses the density of certain vibration modes, which in turn impedes the heat flow.

Heat pulse simulations were also conducted on the Y-junction nanotube. These revealed that the junction at least partially blocked all propagating modes. Furthermore, some asymmetry in heat flow was observed. Traveling waves passed well from the trunk to the branches, but not vice versa. This was attributed the vibrations in traveling waves in the branches being out of phase when they reach the junction. Finally, the inconsistencies in the magnitude and stability of

the waves generated by the heat pulse were attributed to variations in the initial state of the carbon nanotube that get blown up when the heat pulse is applied.

TABLE OF CONTENTS

LIST OF FIGURES

Dedication

I would like to thank my family,

who only expected my best.

CHAPTER ONE

INTRODUCTION

Computers today are constructed with a technology known as Complementary Metal-Oxide-Semiconductor (CMOS) technology, which consists of a network of field-effect transistors patterned onto a silicon wafer using lithographic techniques. The incredible improvements made in this technology over the past several decades are due primarily to the progression of fabrication techniques that allow for CMOS devices to be created at ever-smaller dimensions. Today, these devices have features that can be measured on the scale of tens to hundreds of nanometers. However, the problems with fabricating devices on these scales make it apparent that CMOS devices cannot grow much smaller. Therefore, researchers are attempting to identify a new type of technology that will allow the construction of devices that can be measured on the single-nanometer scale. This exploding area of research is known as nanotechnology.[1]

One of the linchpins of the nanotechnology industry today is the carbon nanotube. Discovered in 1991,[2] the carbon nanotube is a hollow cylinder made entirely of carbon atoms with a radius that can reach less than one nanometer. Shortly after their discovery, several studies were undertaken to determine the electrical properties of these new structures. It was found that some nanotubes are metallic in nature, while others are semiconductors, and that this depends entirely on their chirality.[3] Furthermore, it was found that the band gap of the semiconducting nanotubes is inversely proportional to their radius.[4] Studies of the thermal properties of carbon nanotubes have revealed them to be some of the best thermal conductors known.[5]

The diameter-dependence of the band gap of the semiconducting nanotubes has led researchers to propose and investigate a variety of structures that involve the connection of one nanotube to another. Some of these structures include T-junctions,[6] Y-junctions,[7] and X-junctions.[8] Later, Y-junctions of multi-wall carbon nanotubes were fabricated using a template-based approach that allows the fabrication of many Y-junctions in a single experiment.[9] Theoretical[10] and experimental[11] studies on Y-junction nanotubes have revealed that they behave as electrical rectifiers, much like a diode. However, up to this point no studies on the thermal properties of these structures have been undertaken.

Given their interesting electrical properties and the fact that they can be fabricated in large bundles, it seems important to characterize these Y-junction structures as much as possible. Therefore, the goal of the research described in this thesis is to study the thermal properties of Y-junction carbon nanotubes. To do this, a molecular dynamics approach has been chosen. Molecular dynamics is a method of simulation that determines the time evolution of a set of interacting atoms by integrating their equations of motion. This approach is considered to be classical because the equations of motion are none other than Newton's law, $\vec{F}_i = m_i \vec{a}_i$, for each atom *i* in a system of N atoms. Because this simulation method provides information about the motion of each atom, it is a good one for calculating a variety of thermal properties.

This thesis is organized into six chapters. Chapter 2 describes the structure, electrical and thermal properties of straight and Y-junction carbon nanotubes. A detailed explanation of molecular dynamics can be found in Chapter 3. Chapter 4 describes the methodology and results of steady state heat flow through a Y-junction carbon nanotube. The procedure and results of heat pulse propagation through a Y-junction carbon nanotube are provided in Chapter 5, and conclusions are presented in Chapter 6.

CHAPTER TWO

CARBON NANOTUBES

2.1. Introduction

The growth of carbon nanotubes was first accomplished and reported by Sumio Iijima in 1991.[2] Since that time, a significant amount of effort has been put into the theoretical and experimental study of these structures. The purpose of this chapter is to provide some background information on carbon nanotubes, which will aid in the understanding of subsequent chapters. Specifically, this chapter will discuss the physical structure of straight and Y-junction carbon nanotubes and their resulting electrical and thermal properties.

2.2. Physical Structure

A single-wall carbon nanotube can be viewed as a single sheet of graphite rolled up into a cylinder. Figure 2.1 shows a representation of the 2D hexagonal plane that makes up a graphitic sheet, where the carbon atoms lie at the corners of each hexagon. In this figure, one can see that if point O is connected to point A, and point B is connected to point B', then the sheet will be rolled into a cylindrical structure. However, this is just one of many possible cylindrical orientations that can be constructed. For example, points A and B' could lay directly to the right of points O and B, respectively, which would result in a different orientation of the hexagonal rings on the face of the cylinder.[12]

The vector $\vec{C}_H$, known as the "chiral" vector, is that which uniquely determines the physical structure of a carbon nanotube, and is perpendicular to the tube axis $\vec{z}$. $\vec{C}_H$ can be written in terms of the unit vectors of the hexagonal lattice, $\vec{a}_1$ and $\vec{a}_2$, such that

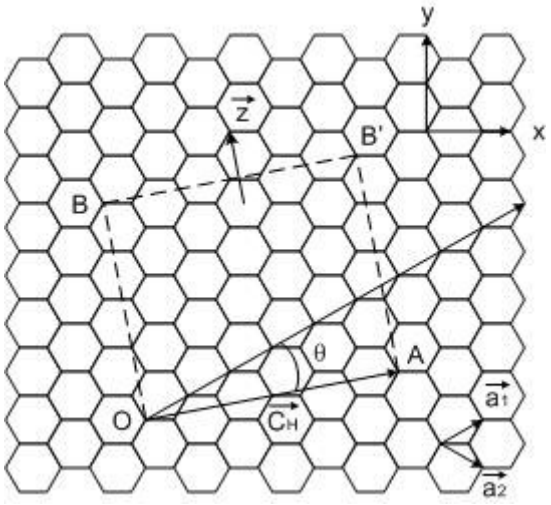

Figure 2.1: The unrolled hexagonal lattice of a nanotube (from Ref. 12).

$\vec{C}_H = n\vec{a}_1 + m\vec{a}_2$. Thus, the integer pair (n,m) is used to completely describe the geometry of a carbon nanotube. Because of the rotational symmetry of the 2D hexagonal lattice, it is only necessary to consider n and m such that $0 \le |m| \le n$. In the case that m = n, the angle θ will be 30^o. In this case, as one moves along the chiral vector, the carbon bonds form an armchair-shaped pattern. Thus, a carbon nanotube of the form (n,n) is known as an armchair nanotube. In the case that m = 0, $\theta = 0^o$ and the bonds along the chiral vector form a zigzag pattern. So, carbon nanotubes of the form (n,0) are known as zigzag nanotubes. In all other cases, $0^o < \theta < 30^o$, and the tubes are known as chiral nanotubes. Figure 2.2 shows an example of each of the three different types of carbon nanotubes.[12] Note the zigzag and armchair patterns at the end rings of the zigzag and arm chair carbon nanotubes. In figure 2.2, all three nanotubes are single-wall carbon nanotubes. There also exist multi-wall carbon nanotubes, which consist of two or more concentric single-wall carbon nanotubes. The focus of study in this research is on single-wall carbon nanotubes.

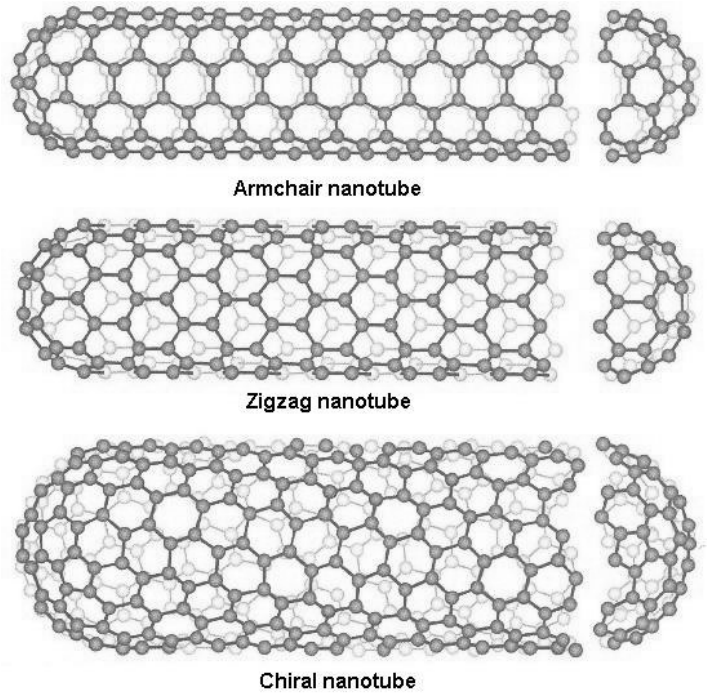

Figure 2.2: Three geometries of carbon nanotubes (from Ref. 12).

The structure of interest in this research, the Y-junction carbon nanotube, was first proposed in 1998.[7] The Y-junction structure consists of a single "trunk" nanotube splitting into two "branch" nanotubes. Figure 2.3 below shows some examples of Y-junction configurations. The structure of the trunk and branches of the Y-junction nanotube is the same as that for a straight single-wall carbon nanotube. The difference in structure lies at the junction, where the continuity of the hexagonal lattice cannot be conserved. To realize the Y-junction, non-hexagonal polygons with 4, 5, 7, or 8 edges must be introduced into the lattice. The number of extra edges introduced into the lattice is known as the bond surplus. Thus, an octagon contributes a bond surplus of +2, while a pentagon contributes a bond surplus of -1. Through an application of Euler's rule for polygons on the surface of a closed polyhedron, Crespi proposed a

rule for the bond surplus of carbon nanotube junctions.[13] His rule was that a junction consisting of N tubes would have a bond surplus of 12(N-2). Thus, a Y-junction should have a bond surplus of 12. However, this surplus can be shared between the two junctions, resulting in a need for 6 extra polygonal edges.[13] In figure 2.3 above, the two Y-junctions on the left contain 6 heptagons, while the one on the right contains 4 heptagons and an octagon.[10]

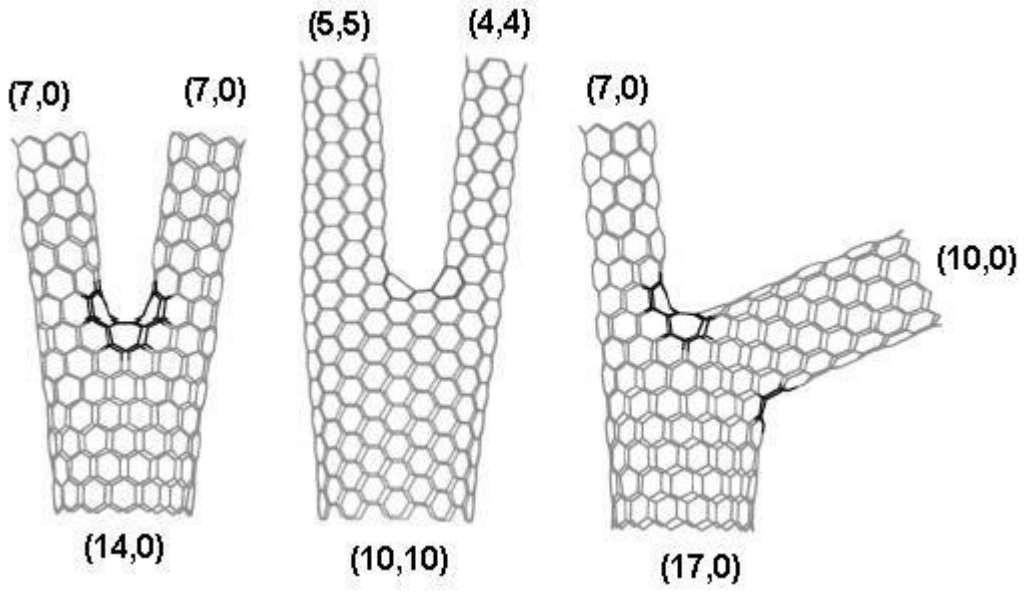

Figure 2.3: Example Y-junction configurations (from Ref. 10).

2.3. Electrical Properties

Soon after their synthesis in 1991, several theoretical studies were undertaken to determine the electrical nature of carbon nanotubes.[3,4,14] These studies found that the electronic structure of carbon nanotubes can be determined starting from that of two-dimensional (2D) graphite. When a plane of graphite is rolled up into a carbon nanotube, periodic boundary conditions are imposed in the circumferential direction described by the chiral vector $\vec{C}_H$, and

the wave vector associated with this direction becomes quantized. Thus, the set of one-dimensional (1D) energy dispersion relations of a carbon nanotube is made up of slices of the 2D energy band structure of graphite.[3] Figure 2.4 shows the reciprocal lattice structure of 2D graphite, and how the carbon nanotube fits into that structure.

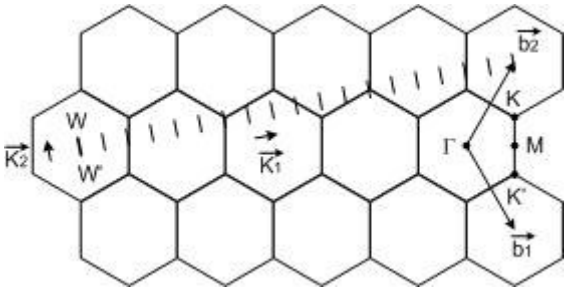

Figure 2.4: Reciprocal lattice diagram of 2D graphite and a carbon nanotube (from Ref. 12).

In this figure, the each hexagon represents a Brillouin zone of 2D graphite. The reciprocal lattice vectors of the 2D graphite are $\vec{b}_1$ and $\vec{b}_2$, while $\vec{K}_1$ and $\vec{K}_2$ are the reciprocal nanotube lattice vectors corresponding to $\vec{C}_H$ and $\vec{z}$, respectively. The line segment WW' represents the first Brillouin zone of a carbon nanotube. Points Γ, M, K, and K' are points of high symmetry in the Brillouin zone of 2D graphite. This figure shows the nature of the quantization of the wave vectors of a carbon nanotube in the form of a series of parallel Brillouin zones. These N distinct wave vectors result in N pairs of 1D energy dispersion relations for the carbon nanotube.[12]

In the energy dispersion relations for 2D graphite, a finite band gap is present along all points in the hexagonal Brillouin zone, except in the corners of the hexagon. At these K points, the band gap drops to zero, resulting in a degenerate energy state. If one of the N wave vectors

of a carbon nanotube passes through a K point, then the 1D energy bands will have a zero energy gap.[12] A finite density of states results from the crossing of two 1D energy bands, which means the carbon nanotube will be metallic in nature. If the wave vectors of a carbon nanotube do not cross through one of the K points, then the 1D energy bands will not overlap and the nanotube will be a semiconductor. The condition for a (n,m) carbon nanotube to be metallic is that $2n + m$ be a multiple of three.[14] An equivalent condition is that $n - m$ be a multiple of three.[12] Thus, a carbon nanotube can be either metallic or semiconducting, depending on its diameter and its chiral angle. Figure 2.5 illustrates this condition.

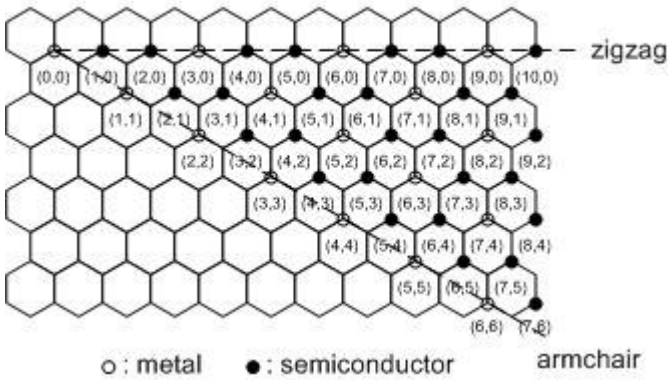

Figure 2.5: Some geometries of carbon nanotubes and their resulting electrical configuration (from Ref. 14).

Another important result is the dependence of the band gap of semiconducting carbon nanotubes on the tube diameter. It has been found that the band gap of a semiconducting nanotube is inversely proportional to its diameter.[12] The electronic behavior and physical structure described above have been verified through the use of scanning-tunneling microscopy (STM).[15]

It has been shown that carbon nanotubes of different geometries exhibit different electrical characteristics. A potentially very useful application of this fact lies in the connection of two or more nanotubes of different geometries. For example, the connection of a metallic nanotube with a semiconducting nanotube will result in a Schottky barrier device, while the connection of two different semiconducting tubes will result in a heterojunction structure.[16] These structures have been shown to exhibit asymmetric electrical properties, both in carbon nanotubes[17] and in traditional CMOS circuits.[18] The usefulness of these structures in present-day circuits underscores how useful carbon nanotubes may be in the development of next-generation electrical devices.

Given that a Y-junction carbon nanotube consists of a connection of two or more different geometries of straight nanotubes, it seems reasonable to assume that this structure will exhibit electrical rectification. Andriotis et al., who used a Green's function formalism to calculate the quantum conductivity of a wide class of Y-junction structures, confirmed this assumption theoretically. They found that the rectification and switching characteristics of these structures depends strongly on their symmetry, and less strongly on the chirality of each branch. Specifically, symmetric Y-junctions with a zigzag trunk always showed perfect rectification, while symmetric Y-junctions without a zigzag trunk exhibited imperfect rectification; an asymmetric I-V characteristic with small leakage currents in cutoff mode. Finally, asymmetric Y-junction structures showed much weaker rectification behavior.[10] Experimental data have also shown the presence of electrical rectification in individual and parallel arrays of Y-junction carbon nanotubes.[11]

2.4. Thermal Properties

One of the more interesting aspects of the thermal characteristics of carbon nanotubes is their thermal conductivity. Thermal conductivity is defined according to

$$\vec{J} = -\kappa \cdot \nabla T \,, \tag{2.1}$$

where $\vec{J}$ is the thermal energy flux, T is the temperature, and κ is the thermal conductivity.[18] The thermal conductivity gives a measure of how much heat will flow through a solid in response to a temperature gradient across the solid. When discussing heat flow, it is useful to identify what exactly is carrying the heat across the temperature gradient. In metals, electrons are the heat carriers. In crystals such as carbon nanotubes, lattice vibrations known as phonons carry heat. When heat conduction is thought of in this way, the thermal conductivity can be written as

$$\kappa = \frac{1}{3} C v l \,, \tag{2.2}$$

where C is the lattice heat capacity, v is the average phonon velocity, and l is the mean free path of the phonons. Heat capacity is a relationship between a change in temperature of the crystal and a corresponding change in the number of phonon modes present. The mean free path describes the average distance a phonon will travel before giving up its energy in some sort of collision.[18]

From equation (2.2), it can be seen that the temperature dependence of the thermal conductivity of a crystal is determined by the temperature dependences of C, v, and l. For the

sake of simplicity, v can be treated as independent of temperature. In three dimensions, the specific heat varies as T^3 at low temperatures, and eventually levels off to a constant value at high temperatures, when all the phonon modes have been excited. At low temperatures, the mean free path of the phonons is relatively long, and is thus limited by the boundaries of the crystal. Therefore, at low temperatures the mean free path is more or less constant, and the thermal conductivity should vary as T^3. As the temperature increases, phonons of shorter wavelengths are excited, and localized defects cause the mean free path to decrease, which causes the thermal conductivity to fall below the T^3 trend. At higher temperatures, the phonons are energetic enough that the majority of their collisions will result in umklapp scattering, which reduces the total phonon momentum and increases the thermal resistance. Thus, at high temperatures the mean free path is the average distance between umklapp collisions. It has been found that l is proportional to 1/T at high temperatures, meaning that the thermal conductivity is also proportional to 1/T at these temperatures.[18] A qualitative plot of this behavior can be seen in figure 2.6. As seen in this figure, the thermal conductivity peaks at a temperature where the crystal size no longer matters but before umklapp collisions start to dominate.

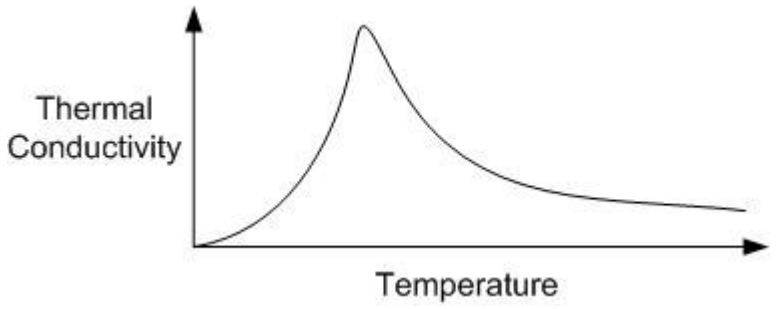

Figure 2.6: Qualitative temperature dependence of the thermal conductivity of crystals.

A variety of studies have been conducted on the thermal conductivity of carbon nanotubes. Hone *et al.* measured the temperature-dependent thermal conductivity of mats of carbon nanotubes. By comparing these values to the electrical conductivity of individual nanotubes and mats of nanotubes, they estimated the room temperature thermal conductivity of an individual nanotube to be in the range 1750-5800 W/m-K.[19] Using a combination of equilibrium and non-equilibrium molecular dynamics simulations, Berber *et al.* predicted the room temperature thermal conductivity of a single (10,10) carbon nanotube to be approximately 6600 W/m-K.[5] Other molecular dynamics simulations predicted this value to be from 1600 W/m-K to 3000 W/m-K.[20,21] While these results show a good deal of variation, they all suggest that the thermal conductivity of carbon nanotubes is at least as high as those of diamond and graphite, making them some of the best thermal conductors known. In later measurements, Hone *et al.* found that the thermal conductivity of an array of single-wall carbon nanotubes peaked at around 400 K.[22] Measurements on multi-wall carbon nanotubes have shown a thermal conductivity that peaks at around 300 K.[23] This is in contrast to diamond and graphite, whose thermal conductivities peak at around 150 K.[22] This indicates that umklapp scattering occurs at much higher temperatures in carbon nanotubes than it does in diamond and graphite. As a result, carbon nanotubes could be significantly better conductors at higher temperatures.

Another interesting thermal property of carbon nanotubes can be seen at very low temperatures. In 1998, Rego and Kirczenow used the Landauer formulation of transport to predict a universal quantum of thermal conductance of $\pi^2 k_B^2 T / 3h$ in 1D quantum wires at very low temperatures.[24] In 2000, Schwab *et al.* experimentally confirmed this value of quantized thermal conductance in silicon nitride nanowires.[25] Given these results, a linear temperature dependence of the thermal conductivity or heat capacity of a material at low temperatures should

indicate the presence of quantized thermal conductance. Hone *et al.* have observed this linear temperature dependence in the thermal conductivity of single-wall carbon nanotubes at temperatures below 30 K.[19] More recently, Hone and his colleagues observed a linear temperature dependence of the specific heat capacity of single-wall carbon nanotubes at temperatures below 8 K.[26] Both of these results indicate the presence of quantized thermal conductance in single-wall carbon nanotubes.

Given their structure, Y-junction nanotubes can be expected to exhibit similar thermal characteristics to straight carbon nanotubes. However, the presence of the junction in the middle of the structure suggests that some fundamental differences between their thermal properties should exist. Up to this point no studies on the thermal properties of Y-junction carbon nanotubes have been conducted.

CHAPTER THREE

MOLECULAR DYNAMICS

3.1. Introduction

Molecular dynamics simulation is a classical approach to modeling systems of atoms and molecules. It makes use of Newton's laws of motion and an accurate interatomic potential to determine the motion of each atom or molecule in the system. With detailed knowledge of the motion of each particle in the system, a variety of useful information can be determined. In the sections below, the general approach used in molecular dynamics is discussed, as are some of the more specific calculations made in the course of this research.

3.2. General Method

As stated above, the molecular dynamics approach is classical in the sense that it makes use of Newtonian mechanics to determine the behavior of the system. In order to determine the forces acting on each atom in a particular system, an interatomic potential function is used. The potential function defines the potential energy between a pair of atoms as a function of their distance from one another. Thus, the potential function can be written as $U(r_{ij})$, where r_{ij} represents the distance between the i^{th} and j^{th} atoms in the system under investigation. For the sake of simplicity in notation, this is rewritten as U_{ij}. Once the potential energy between a pair of atoms is known, the force between the two atoms can be found by taking the gradient of the potential function with respect to their distance: $\vec{F}_{ij} = -\nabla U_{ij}$. Then, the net force on a particular atom can be found by summing the forces due to all other atoms in the system: $\vec{F}_i = -\sum_{j \neq i} \nabla U_{ij}$.

Once the net force on a particular atom is known, its acceleration at a particular instant in time is easily derived using Newton's second law of motion:

$$\vec{a}_i = \vec{F}_i / m_i \tag{3.1}$$

In equation (3.1), m_i is the mass of the atom in question.[27]

Above it was stated that the force on a particular atom is determined as a sum of the forces due to all the other atoms in the system. This is the case because most potential functions have an infinite range. In practice, however, the large number of atoms in many systems makes this approach computationally unfeasible. Therefore, it is necessary to limit the number of contributors to the force on a particular atom. One way to do this is to introduce a cutoff term to the potential function that limits its effect to a specific range. Thus, any atoms separated by more than this range would not interact with one another. The potential function used in this research includes a cutoff term. Another method used in these simulations is the nearest-neighbor method. The potential function used in this research describes the potential energy between a pair of bonded carbon atoms. Thus, it should not be applied to a pair of carbon atoms that are not directly bonded together. A given atom in a carbon nanotube can be bonded with only its nearest neighbors. Therefore, a list of nearest neighbors for each atom is maintained, which significantly limits the number of pair-wise interactions that must be calculated.

To account for the movement of the atoms in the system over time, the simulation is broken into a series of sequential time steps. At each time step the details of the movement of each atom are calculated. This is usually done using a predictor-corrector scheme. In this scheme, a Taylor series expansion is used to predict the position, velocity, acceleration, and

higher-order terms of each atom for the next time step, based on their values at the current time step. In the equations below, the expansion of terms in the Taylor series to third order can be seen.[28]

$$r(t+\Delta t) = r(t) + \dot{r}(t)\cdot\Delta t + \frac{1}{2!}\ddot{r}(t)\cdot\Delta t^2 + \frac{1}{3!}\dddot{r}(t)\cdot\Delta t^3 \tag{3.2}$$

$$\dot{r}(t+\Delta t) = \dot{r}(t) + \ddot{r}(t)\cdot\Delta t + \frac{1}{2!}\dddot{r}(t)\cdot\Delta t^2 \tag{3.3}$$

$$\ddot{r}(t+\Delta t) = \ddot{r}(t) + \dddot{r}(t)\cdot\Delta t \tag{3.4}$$

$$\dddot{r}(t+\Delta t) = \dddot{r}(t) \tag{3.5}$$

Recall that the velocity is the time-derivative of the position r(t), the acceleration is the second time-derivative of the position, and the jerk is the third time-derivative of the position. Once the position, velocity, acceleration, and jerk have been predicted for the next time step, they are used to calculate the relevant properties of the system at that time step, such as temperature and energy. The calculation of these and other parameters will be discussed in a later section.

Due to the fact that the Taylor series is an infinite series, the results of equations (3.2)-(3.5) will have slight errors due to the truncation of the series after the third-order term. If left uncorrected over many time steps, these truncation errors can build up to significant values, resulting in inaccurate data. Therefore, it is necessary to correct the values predicted in equations (3.2)-(3.5). There are several ways to do this. The method used in this research is described below in section 3.4. After the predicted values have been corrected, they can then be applied to equations (3.2)-(3.5) again to predict the movement of the atom for the next time step.

This process continues until the target number of time steps has been reached. A schematic of this process can be seen in figure 3.1 below.

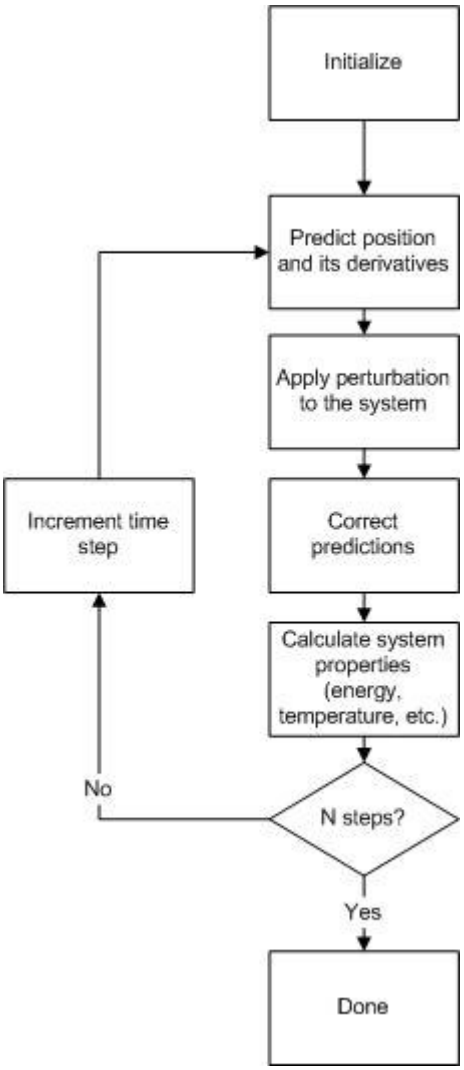

Figure 3.1: High-level process of molecular dynamics simulation.

3.3. The Tersoff-Brenner Interatomic Potential

In the section above, the role of the interatomic potential was discussed. Tersoff first developed the basis for the potential used in this research for the simulation of covalent silicon.[29]

The potential he used took the form $U_{ij} = f_C(r_{ij}) \cdot \left(a_{ij} \cdot f_R(r_{ij}) - b_{ij} \cdot f_A(r_{ij})\right)$, and describes the potential energy between a pair of covalently bonded atoms. In this expression, f_R represents the repulsive force between two bonded atoms, f_A represents the attractive force, and f_C represents the cutoff term. When a_{ij} and b_{ij} are taken to be constants, this is a standard two-body potential. However, because there are a variety of bonding geometries available to covalent silicon, this potential cannot accurately represent all of those forms. Therefore, Tersoff updated these parameters such that they both depend on the bond order - the number of available bonding neighbors. This allowed for a simple potential to simultaneously represent the various bonding geometries that can occur in silicon.[29] In a later paper, Tersoff calculated the parameters necessary to apply his potential to amorphous carbon.[30]

While Tersoff's bond-order potential appeared to be accurate and flexible, Brenner discovered some inherent problems when the potential was applied to certain double-bonding situations in carbon.[31] Therefore, he added an adjustment to the bond-order terms to account for those problems. The combination of Tersoff's bond-order potential for carbon and Brenner's subsequent adjustment is known as the Tersoff-Brenner interatomic potential, and is the one used in this study of carbon nanotubes.

3.4. The Nordsieck-Gear Predictor-Corrector Method

In the section describing the general method of molecular dynamics, it was noted that the predicted values describing the position and movement of each atom needed correction before a new prediction could be made. This research makes use of the Nordsieck predictor-corrector scheme. This scheme makes its predictions based on a slightly modified form of equations (3.2)-(3.5):

$$r(t+\Delta t) = r(t) + \dot{r}(t)\cdot\Delta t + \frac{1}{2!}\ddot{r}(t)\cdot\Delta t^2 + \frac{1}{3!}\dddot{r}(t)\cdot\Delta t^3 \tag{3.6}$$

$$\dot{r}(t+\Delta t)\cdot\Delta t = \dot{r}(t)\cdot\Delta t + \ddot{r}(t)\cdot(\Delta t)^2 + \frac{1}{2!}\dddot{r}(t)\cdot\Delta t^3 \tag{3.7}$$

$$\ddot{r}(t+\Delta t)\cdot\frac{(\Delta t)^2}{2!} = \ddot{r}(t)\cdot\frac{(\Delta t)^2}{2!} + \dddot{r}(t)\cdot\frac{(\Delta t)^3}{2!} \tag{3.8}$$

$$\dddot{r}(t+\Delta t)\cdot\frac{(\Delta t)^3}{3!} = \dddot{r}(t)\cdot\frac{(\Delta t)^3}{3!} \tag{3.9}$$

Then, the vector z(t) and the matrix A are defined such that

$$z(t) = \begin{bmatrix} r(t) \\ \dot{r}(t)\cdot\Delta t \\ \ddot{r}(t)\cdot\frac{(\Delta t)^2}{2!} \\ \dddot{r}(t)\cdot\frac{(\Delta t)^3}{3!} \end{bmatrix} \text{ and } A = \begin{bmatrix} 1 & 1 & 1 & 1 \\ 0 & 1 & 2 & 3 \\ 0 & 0 & 1 & 3 \\ 0 & 0 & 0 & 1 \end{bmatrix}. \tag{3.10}$$

Thus, the prediction consists of the matrix equation $z^P(t+\Delta t) = A\cdot z(t)$.[28] The superscript P indicates that the values are the predicted values.

For correction, the Nordsieck formulation makes a comparison between the acceleration calculated in equation (3.4), $\ddot{r}(t+\Delta t)$, and that calculated from the interatomic potential in equation (3.1), $a(t+\Delta t)$. Then, the error can be defined as $e(t) = \left[a(t+\Delta t) - \ddot{r}(t+\Delta t)\right]\frac{(\Delta t)^2}{2!}$.

To correct this error, the results of equations (3.6)-(3.9) are scaled by a value proportional to the error in the acceleration, such that[28]

$$z(t+\Delta t) = z^P(t+\Delta t) + e(t)\cdot\begin{bmatrix} 1/6 \\ 5/6 \\ 1 \\ 1/3 \end{bmatrix}. \tag{3.11}$$

3.5. Calculation of System Properties

This section details the calculation of the various system properties used in this research on Y-junction carbon nanotubes.

3.5.1. Kinetic Energy

Because the velocity of each atom is known at every time step, the total kinetic energy of a group of N atoms at a specific point in time is just the sum of their individual kinetic energies: $E_{group} = \sum_{i=1}^{N} \frac{1}{2} m_i v_i^2$. The average kinetic energy per atom is obtained by dividing by the total number of atoms in the group: $E_{avg} = \frac{1}{N} \sum_{i=1}^{N} \frac{1}{2} m_i v_i^2$.

3.5.2. Temperature

According to the law of equipartition,[32] temperature is proportional to the average atomic kinetic energy. In three dimensions $E_{avg} = \frac{3}{2} k_B T$, where k_B is Boltzmann's constant. Thus, using the calculation of average energy in section 3.5.1, the temperature of a group of atoms is $T = \frac{2E_{avg}}{3k_B}$.

It should be noted that this definition of temperature applies to the high temperature regime, where quantum effects are not important. At lower temperatures, this definition is not necessarily accurate. However, Che *et al.* have argued that the classical heat flux autocorrelation can successfully replace its quantum counterpart, even in the low temperature range.[21] It is possible that this argument can be extended to the definition of temperature at low temperatures.

3.5.3. Velocity Autocorrelation Function

As discussed in section 3.2, molecular dynamics simulations give the position, velocity, and acceleration of the atoms in a given system over time. Thus it is possible to use molecular dynamics to study the time evolution of a system. Time correlation functions provide a way to do this. To develop the concept of a time correlation function, let p(t) and q(t) denote all the momenta and spatial coordinates of the system in question. Next, define a pair of variables A and B that are dependent on p(t) and q(t). Then, it is possible to say that $A(p(t),q(t)) = A(p(0),q(0);t) = A(t)$ and $B(p(t),q(t)) = B(p(0),q(0);t) = B(t)$. The time correlation function of variables A and B is defined as:

$$C_{AB}(t) = \langle A(0)B(t)\rangle = \iint dpdqA(p,q;0)B(p,q;t)f(p,q)\,. \tag{3.12}$$

In equation (3.12), f(p,q) represents the equilibrium distribution of p and q. When variables A and B are equal, this function is referred to as an autocorrelation function. When the variables are vector-valued quantities, a dot product is used in equation (3.12). For example, the velocity autocorrelation function described below is written as $C_{vv}(t) = \langle \vec{v}(0)\cdot\vec{v}(t)\rangle$. Another important feature of this function is that taking its Fourier transform can reveal important frequency-dependent information about the variables used in the function.[33]

Equation (3.12) can very difficult to calculate analytically. In the case of the velocity autocorrelation function, $C_{vv}(t)$, the dependence of the velocities on position and momentum can be very complicated, and will involve some form of equations (3.2)-(3.5) as well as the interatomic potential. Fortunately, an analytical solution is not required when working with molecular dynamics. Since the velocities are already known at each time step, the dependence of

the velocity on p(t) and q(t) does not need to be considered; it has already been included in the calculation. Thus, the velocity can be treated solely as a function of time, making the calculation of $C_{vv}(t)$ fairly straightforward.

Using the argument in the previous paragraph, the velocity autocorrelation function can be written $C_{vv}(t_k) = \vec{v}(0) \cdot \vec{v}(t_k)$. The subscript k has been included because of the quantization of time into discrete steps. This expression refers to the autocorrelation function of the velocity of a single atom. However, it is useful to consider the average motion of a group of atoms in a system. In addition, the autocorrelation function does not need to start at time zero. Rather, it can start at any reference time during the course of the simulation. Therefore, the velocity autocorrelation function can be updated to $C_{vv}(t_k) = \frac{1}{M}\sum_{i=1}^{M} \vec{v}_i(\tau) \cdot \vec{v}_i(\tau + t_k)$, where M is the number of atoms under investigation and τ is the reference time. Another convention that is usually taken in molecular dynamics simulations is to normalize the velocity autocorrelation function with respect to its initial value:

$$\tilde{C}_{vv}(t_k) = \frac{C_{vv}(t_k)}{C_{vv}(0)} = \frac{\frac{1}{M}\sum_{i=1}^{M} \vec{v}_i(\tau) \cdot \vec{v}_i(\tau + t_k)}{\frac{1}{M}\sum_{i=1}^{M} \vec{v}_i(\tau) \cdot \vec{v}_i(\tau)}. \tag{3.13}$$

Finally, during the course of a simulation it is possible to calculate several normalized velocity autocorrelation functions concurrently, with each starting at a different reference time. These separate functions are then averaged together to obtain an overall result. Denoting a

particular autocorrelation function with starting time τ_j as $\tilde{C}_{vv}^{j}(t_k)$, the overall velocity autocorrelation function can be written as

$$\tilde{C}_{vv}(t_k) = \frac{1}{N}\sum_{j=1}^{N}\tilde{C}_{vv}^{j}(t_k) = \frac{1}{N}\sum_{j=1}^{N}\frac{\sum_{i=1}^{M}\vec{v}_i(\tau_j)\cdot\vec{v}_i(\tau_j + t_k)}{\sum_{i=1}^{M}\vec{v}_i(\tau_j)\cdot\vec{v}_i(\tau_j)}. \qquad (3.14)$$

Equation (3.14) provides an average picture of the time-dependent motion of a particular group of atoms in the system under investigation. An example of the time evolution of one of these functions can be seen in figure 3.2. This figure shows the velocity autocorrelation function of a (14,0) carbon nanotube. The overall function was calculated for t_k up to 1024 time steps, and was averaged over N = 32 separate functions, each started 64 time steps apart.

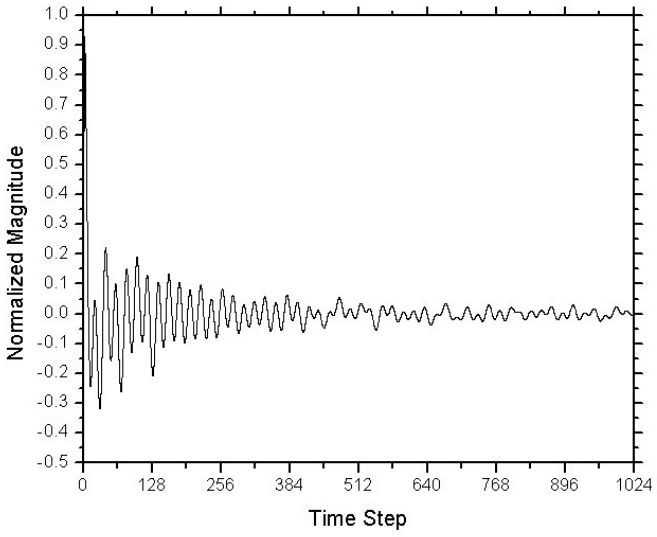

Figure 3.2: Velocity autocorrelation function of a (14,0) carbon nanotube.

As stated above, the Fourier transform of time correlation functions can reveal important information about the variables included in the function. In the case of the velocity autocorrelation function, the Fourier transform represents the spectral density of the atomic motions, and can be used to determine which modes of vibration are dominant in a given system. Some examples of this analysis can be found in Chapter 4.

3.5.4. Thermal Conductivity

Several approaches to calculating the thermal conductivity of a system using molecular dynamics simulations have been proposed.[34-36] The details of the approach used in this research can be found in Chapter 4, which discusses the thermal properties of Y-junction carbon nanotubes under steady state conditions.

CHAPTER FOUR

STEADY STATE HEAT FLOW

4.1. Introduction

As stated in Chapter 2, up to this point no studies have been conducted on the thermal properties of Y-junction carbon nanotubes. In this chapter, a molecular dynamics approach to the modeling of steady state heat flow in a Y-junction carbon nanotube is presented. The goal is to calculate the thermal conductivity of the Y-junction structure, and determine how it might differ from that of a straight carbon nanotube. In the following sections, the method for determining the thermal conductivity is described, the results are presented, and an analysis of these results is provided.

4.2. Methodology

To model the dynamics of the atoms within the Y-junction nanotube, a molecular dynamics approach has been chosen, with the Tersoff-Brenner bond order potential for the C-C bond as the potential interaction function.[30,31] Within the molecular dynamics paradigm, a variety of approaches to the calculation of thermal conductivity have been examined.[34-36] The approach discussed by Oligschleger and Schön,[34] and implemented in straight carbon nanotubes by Osman and Srivastava,[20] splits the nanotube into a series of equal "slabs" of atoms. Two of the slabs are thermally regulated to enforce a temperature gradient upon the system, as shown in figure 4.1.

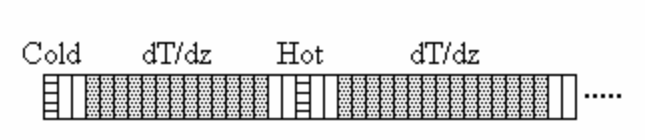

Figure 4.1: Molecular dynamics setup for calculating the thermal conductivity of a straight carbon nanotube. The ellipses indicate that periodic boundary conditions are applied.

The temperature of each of these slabs is regulated by a scaling of the velocities of the atoms within the slab. The velocities are scaled according to

$$v_{i,new} = v_{i,old} \cdot \sqrt{\frac{T_{control}}{T_{current}}}, \tag{4.1}$$

where $T_{control}$ is the desired temperature of the slab, and $T_{current}$ is the current slab temperature. In this approach, $T_{control} = T_{amb} + \Delta T$ for the hot slab and $T_{control} = T_{amb} - \Delta T$ for the cold slab, where T_{amb} is the initial temperature of the solid. The change in energy of the controlled slabs at each time step is given by

$$\Delta E_{slab} = \frac{1}{2} m \sum_{i=1}^{N} \left(v_{i,new}^2 - v_{i,old}^2 \right), \tag{4.2}$$

where N is the number of atoms in the slab, m is the mass of each atom, and $v_{i,new}$ is calculated according to equation (4.1). The heat flux density at the n^{th} time step of the simulation is calculated by taking an average of the net energy added at each previous time step:

$$J(n) = \frac{1}{A} \cdot \frac{\sum_{j=1}^{n} \left| \Delta E_{hotslab}(j) + \Delta E_{coldslab}(j) \right|}{n \cdot \Delta t}, \tag{4.3}$$

where the $\Delta E_{slab}(j)$ come from equation (4.2), Δt is the time associated with each simulation step, and A is the cross-sectional annular ring area of the nanotube.[20] After a large number of simulation steps, an equilibrium value of the heat flux density is obtained. The temperature gradient, dT/dz, is found by applying a linear fit to the temperatures of the slabs in the gray region in figure 4.1, and the thermal conductivity at the nth simulation step is the quotient of the heat flux density and the temperature gradient:

$$\kappa(n) = \frac{J(n)}{dT / dz}, \tag{4.4}$$

where J(n) is given by equation (4.3). One final note that should be made from figure 4.1 is that periodic boundary conditions have been applied in order to eliminate edge effects.[34]

To investigate the thermal conductivity of the Y-junction nanotube, an algorithm similar to that described by Oligschleger and Schön has been chosen. The setup is similar to that shown in figure 4.1, except for the fact that, due to its linear asymmetry, periodic boundary conditions cannot be applied to the Y-junction configuration. Therefore, an alternate setup has been chosen, and can be seen in figure 4.2. In this setup, the black slabs labeled "Fixed" have atoms that are fixed in space in order to prevent tube drift and oscillations during the simulation. The slabs labeled "Hot" and "Cold" are the velocity-scaled slabs, whose temperatures are controlled as described in equation (4.1). The energy flux density at the nth simulation step is calculated in the

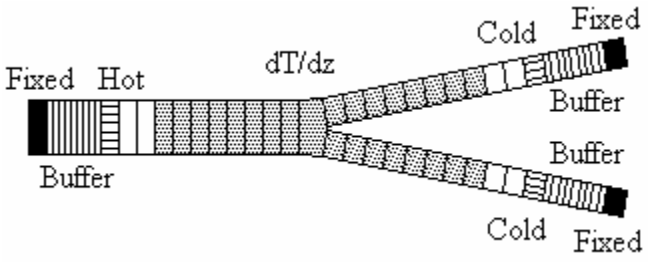

Figure 4.2: Molecular dynamics setup for calculating the thermal conductivity of the Y-junction nanotube.

same manner as in equation (4.3), but with an extra term to account for the fact that there are two cold velocity-scaled slabs instead of just one:

$$J(n) = \frac{1}{A} \cdot \frac{\sum_{j=1}^{n} \left| \Delta E_{hot}(j) + \Delta E_{cold1}(j) + \Delta E_{cold2}(j) \right|}{n \cdot \Delta t}. \tag{4.5}$$

The slabs labeled "Buffer" act as thermal reservoirs, in an attempt to minimize edge effects by providing a buffer between the velocity-scaled slabs and the fixed tube ends. The temperature of these buffer slabs is the same as that of their adjacent velocity-scaled slabs. However, their temperature is maintained through a more realistic application of friction and random forces, which satisfy the fluctuation-dissipation theorem through the Langevin dynamics approach. In order to obtain a single temperature gradient dT/dx for the entire structure, the positions and temperatures of corresponding slabs in the two branches were averaged before a linear fit was calculated.

In the algorithm described above, a temperature gradient is imposed by a set of thermal reservoirs and the resultant heat flux is measured to determine the thermal conductivity of the Y-junction nanotube. Müller-Plathe has proposed carrying out this process in the reverse order. In

his scheme, the velocity of the hottest (most energetic) atom in the cold slab is exchanged with the velocity of the coldest atom in the hot slab at regular intervals. This has the effect of imposing a known heat flux on the system. Once a steady state has been reached, the resulting temperature gradient is measured to determine the thermal conductivity.[35]

The velocity-exchange approach has a couple advantages. First, because the temperature gradient is a quantity that converges much more quickly than heat flux, this method requires much fewer time steps than the thermal reservoir method used in this research. Second, the resultant temperature gradient tends to be smaller than in the thermal reservoir approach. Because the thermal conductivity of a material is normally temperature-dependent, a large temperature gradient can result in a large variation in the local thermal conductivity across the system. A small temperature gradient allows a more accurate measure of the system's overall thermal conductivity.[35] However, the application of this method in the Y-junction structure is problematic because of the presence of two cold reservoirs and only one hot reservoir. It would be difficult to ensure that the two branches are maintained at the same temperature.

Another approach makes use of a fictitious force field applied along the direction of heat flow. This fictitious field imposes a heat flux on the system under investigation by forcing hot and cold atoms in opposite directions. This approach has the advantage of inducing no temperature gradient, and as the fictitious field gets small, a very accurate value of thermal conductivity can be obtained. However, this method relies on the assumption of periodic boundary conditions, which cannot be applied to the Y-junction structure.

As stated earlier, the linear asymmetry of the Y-junction structure precludes the application of periodic boundary conditions to the system. The buffer slabs were added in an attempt to provide a shield from edge effects, but it is still possible that the tube ends could have

an effect on the heat flow within the system. Furthermore, the alternate methods described above may provide more accuracy than the method chosen. Thus, absolute magnitude of the thermal conductivity may not be as accurate as it could be. The chosen method, however, is reasonable for identifying trends and relative magnitudes of heat transport in a branched nanotube structure in comparison with straight nanotubes with or without defects.

4.3. Results

For the molecular dynamics simulations, a Y-junction with a (14,0) zigzag trunk splitting into two (7,0) zigzag branches was used. There were 35 slabs in each of the three branches, and one slab in the middle connecting them, for a total of 106 slabs including 3980 atoms. With a length of 4.26 Å per slab, each branch in the tube measured about 15 nm long. This is long enough for a qualitative comparison of thermal transport in branched and straight carbon nanotubes, but not for absolute values of thermal conductivity. The thermal conductivity simulation was run at base temperatures of 200 K to 400 K in increments of 50 K. A temperature differential of ± 50 K between the trunk and the two branches was used in each case. Two simulations were run for each base temperature, one with a hot trunk and cold branches (designated as "forward" heat flow), and one with a cold trunk and hot branches ("reverse" heat flow). For comparison, a (14,0) straight nanotube of 71-slab length was also run at these temperatures. The straight tube was configured in a manner similar to that shown in figure 4.2, with the fixed ends, buffer slabs and velocity-scaled slabs. Each simulation was run for 200,000 time steps, with the heat flux density averaged over the last 100,000 time steps. For these simulations, the time step was 0.5 fs, and the cross-sectional area was calculated based on an annular ring width of 3.4 Å.[20]

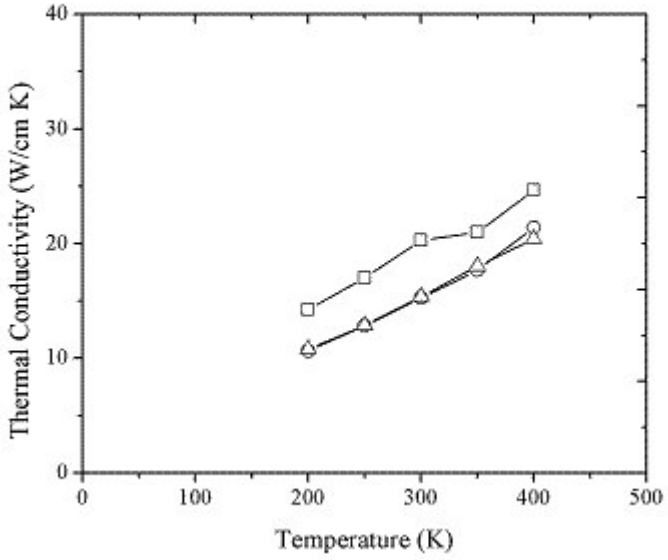

Figure 4.3: Temperature dependence of the thermal conductivity. The squares represent the straight (14,0) nanotube, the triangles represent the forward heat flow configuration of the y-junction tube, and the circles represent the reverse heat flow configuration of the y-junction tube.

The results for the thermal conductivity of the nanotubes are summarized in figure 4.3. For temperatures up to 400 K, there is no significant difference between the "forward" and "reverse" heat conductivity of the Y-junction carbon nanotube. This is in contrast to the theoretical result indicating significant electrical rectification in the same Y-junction nanotube configuration.[10] Additionally, the thermal conductivity exhibits an increase with temperature similar to what has been reported experimentally[19] for straight carbon nanotubes. Figure 4.3 also indicates that the thermal conductivity of the straight (14,0) nanotube was consistently larger than that of the Y-junction structure.

The heat flux density results are shown in figure 4.4. This figure indicates that the forward and reverse energy flux values of the Y-junction nanotube are almost exactly the same

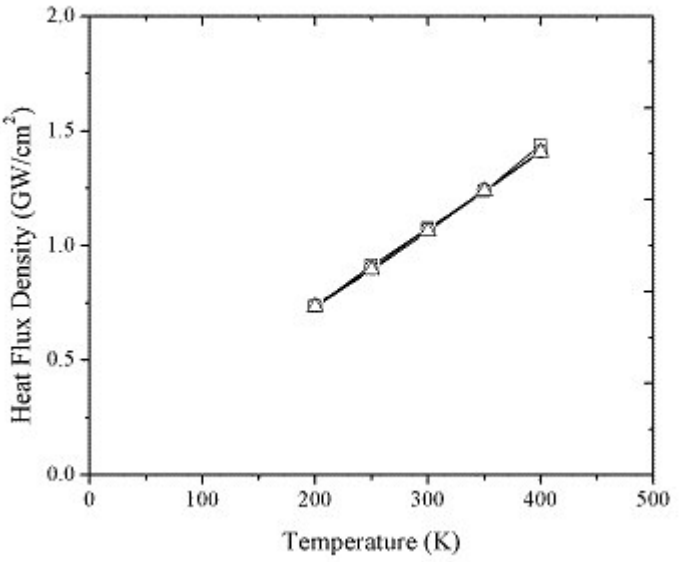

Figure 4.4: Temperature dependence of the heat flux density. The squares represent the straight (14,0) nanotube, the triangles represent the forward heat flow configuration of the y-junction tube, and the circles represent the reverse heat flow configuration of the y-junction tube.

for all temperatures. Furthermore, these flux values are essentially identical to those of the straight (14,0) nanotube. Given this, it stands to reason that the differences in thermal conductivity between the Y-junction and the straight nanotubes are due to differences in the temperature gradient. Figure 4.5 shows the values of the temperature gradient obtained, and indicates that the Y-junction tube has a higher temperature gradient than the straight (14,0) tube for all temperatures.

Figure 4.6a shows the temperature profile along the straight (14,0) nanotube at 300 K and figure 4.6b shows that of the Y-junction nanotube, also at 300 K. These figures help to explain the reason why the Y-junction nanotube has a higher temperature gradient than the straight nanotube. As seen in figure 4.6b, the Y-junction nanotube exhibits a sharp discontinuity in the temperature profile at slab positions 35-37, where the trunk splits into the two branches. No such

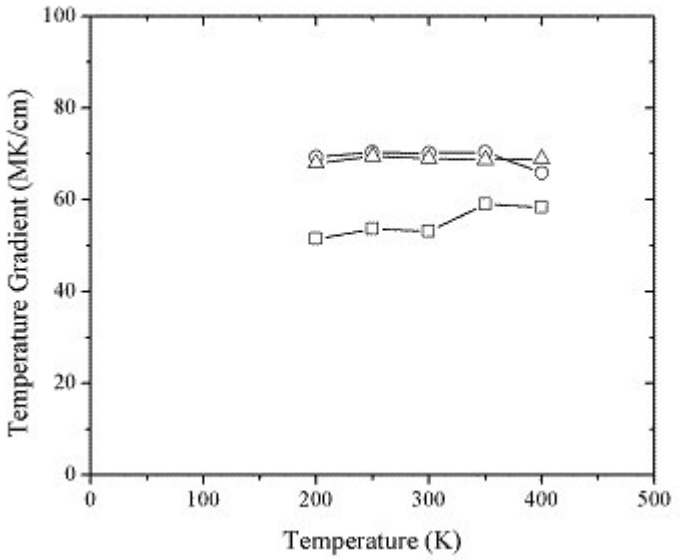

Figure 4.5: Temperature dependence of the temperature gradient. The squares represent the straight (14,0) nanotube, the triangles represent the forward heat flow configuration of the y-junction tube, and the circles represent the reverse heat flow configuration of the y-junction tube.

discontinuity in the temperature profile exists for the straight tube. This small region of relatively large temperature gradient is a result of the presence of high resistance to heat flow at the junction. This high resistance, in turn, results in the lower values for the thermal conductivity of the Y-junction nanotube.

Discontinuities in the temperature profile have been observed in the context of molecular dynamics simulations before. Using a non-equilibrium molecular dynamics approach, Maiti *et al.* have investigated the heat flow across crystal grain boundaries. They have reported a similar temperature profile across a grain boundary in a silicon crystal.[37] Maruyama *et al.* have reported seeing a jump in the temperature profile of a carbon nanotube heterojunction consisting of a (12,0) tube connected to a (6,6) tube.[38] In each of these cases, the jump in the temperature profile seems to be associated with the presence of discontinuities or defects in the crystal lattice

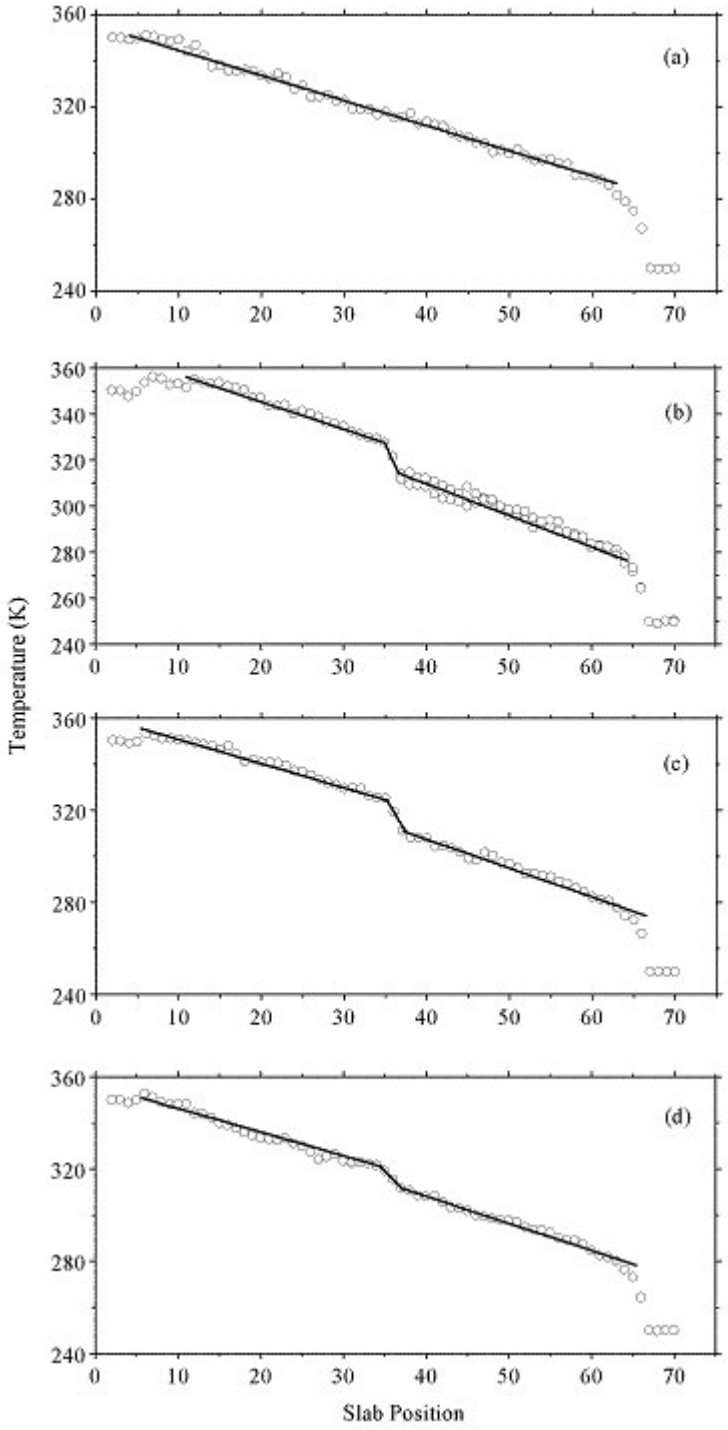

Figure 4.6: Temperature profiles of (a) the straight (14,0) nanotube, (b) the Y-junction nanotube, (c) the straight (14,0) nanotube with vacancy defects, and (d) the straight (14,0) nanotube with a Stone-Wales (5,7,7,5) defect. Fit lines have been added to show the slope in each region.

under investigation. These defects act as additional scattering centers and result in a region of large temperature gradient, which translates to a reduction in the thermal conductivity of the crystal. Che *et al.* have reported his type of behavior, with theoretical calculations that indicate an inverse relationship between the number of defects in a crystal and the thermal conductivity of the crystal.[21] In the Y-junction tube examined in this paper, lattice defects are present in the form of six heptagonal carbon rings at the junction point.[10]

In order to understand the origin of the discontinuity at the Y-junction, two types of defects were intentionally introduced into the middle of two straight (14,0) nanotubes. The first type of defect was in the form of atomic vacancies and was created by the removal of two atoms from the middle slab of the tube. The second type of defect was a Stone-Wales (5, 7, 7, 5) defect, where four hexagons are changed into two pentagons and two heptagons. These tubes were then run through the simulation at 300 K, with the usual $\pm$ 50 K hot and cold slabs applied. The resulting temperature gradient of the tube with vacancies can be seen in figure 4.6c, while that of the tube with the Stone-Wales defect can be seen in figure 4.6d. As seen in these figures, the temperature profile of the straight nanotube with two vacancies is very similar to that of the Y-junction, while the temperature profile of the tube with the Stone-Wales defect exhibits a discontinuity that is much less pronounced. Additionally, the resulting values of the temperature gradient and the thermal conductivity of the (14,0) tubes with defects were calculated. The nanotube with vacancies had the same thermal conductivity and temperature gradient as those obtained for the Y-junction nanotube at the same temperature. The nanotube with the Stone-Wales defect had a smaller temperature gradient and thus a larger thermal conductivity than the Y-junction tube, but a smaller thermal conductivity than the defect-free (14,0) tube. Che *et al.* noted that Stone-Wales defects have a less significant effect on thermal conductivity than

vacancies,[21] which is consistent with the smaller temperature profile discontinuity seen in figure 4.6d. They concluded that the Stone-Wales defects were less severe because they do not change the bonding configuration of the lattice and thus induce less structural deformation. The greater amount of structural deformation in the Y-junction nanotube suggests that it will exhibit a more significant discontinuity in the temperature profile.

In an attempt to clarify the reason behind the presence of the jump in the temperature profiles, the phonon spectra of the nanotubes in question were investigated. The phonon spectra were found by taking the Fourier transform of the velocity autocorrelation functions of each tube, which were calculated over 1024 time steps in the molecular dynamics simulations. Of interest were the frequency distributions of atomic vibrations along two different directions. Axial phonons and radial phonons represent vibrations parallel and perpendicular to the nanotube axis, respectively. Therefore, two autocorrelation functions were calculated, one using only the component of the atomic velocities parallel to the nanotube axis, and one using only velocity components perpendicular to the nanotube axis.

Figure 4.7a shows the axial phonon spectrum of the atoms in a single defect-free slab in the (14,0) nanotube. A primary peak exists at around 50 THz, with a lesser peak at about 20 THz. In figure 4.7b, the axial phonon spectrum of the atoms in the slab with vacancies in the (14,0) tube is shown. Again, the phonon density peaks at about 20 THz and 50 THz. However, the magnitude of the 50 THz peak is about 15% smaller than that of the defect-free slab. Figure 4.7c shows the axial phonon spectrum of the atoms in the slab with the Stone-Wales defect. The magnitude of the 50 THz peak is about 16% smaller than that of the defect-free slab. Finally, figure 4.7d shows the axial phonon spectrum of the atoms of slab 35 in the Y-junction tube. Slab 35 is the slab in the (14,0) trunk of the Y-junction that is adjacent to the middle “hub” slab.

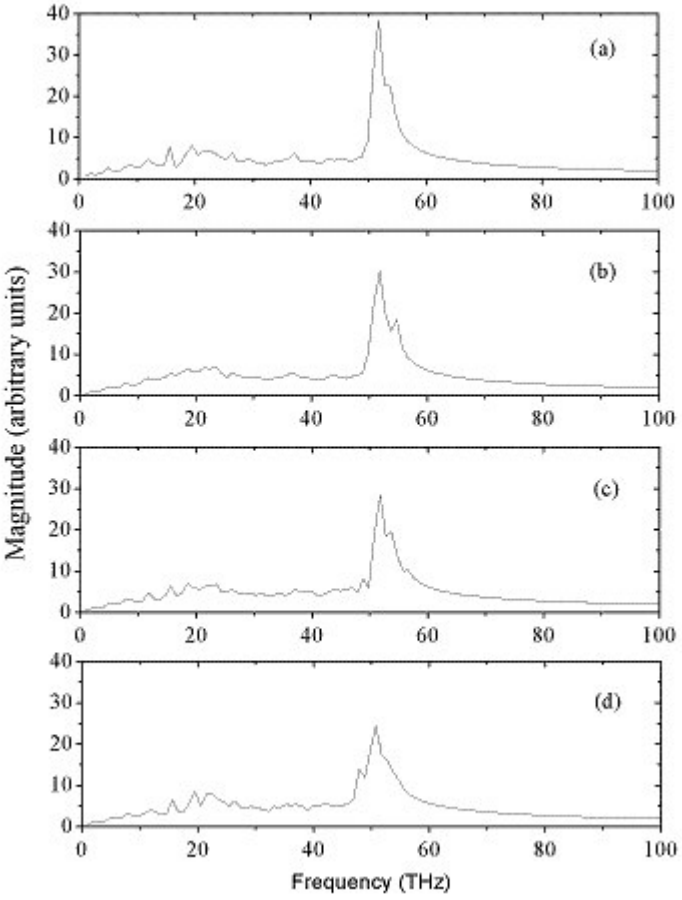

Figure 4.7: Axial phonon spectra of (a) the straight (14,0) nanotube, (b) the straight (14,0) tube slab with vacancy defects, (c) the straight (14,0) nanotube slab with a Stone-Wales (5,7,7,5) defect, and (d) Y-junction slab 35. These spectra represent atomic vibrations parallel to the tube axis.

Moving from left to right along the temperature profile of the Y-junction tube in figure 4.6b, one can see that slab 35 is where the first significant discontinuity in the temperature drop occurs. Again, peaks in the phonon density of the atoms in this slab exist at 20 THz and 50 THz. In this case the magnitude of the 50 THz peak is about 30% smaller than that in the defect-free (14,0) slab. Similar results were obtained for the radial phonon spectra of the nanotubes. The magnitudes of the 50 THz peaks in the radial phonon spectra of the Y-junction and (14,0)

nanotube with vacancies were both 7% smaller than that of the defect-free (14,0) nanotube, while the peak in the tube with the Stone-Wales defect was 20% smaller.

4.4. Discussion

The steady state heat flow properties of a Y-junction nanotube consisting of a (14,0) trunk splitting into two (7,0) branches have been investigated using molecular dynamics simulations. Thermal transport under steady state does not show any anisotropy with respect to the direction of the heat flow, which is in contrast to the evidence of electrical rectification in the same structure. In their calculations, Andriotis *et al.* accounted for the effects of quantum states on electrical conduction in Y-junction carbon nanotubes through an application of Green's functions.[10] Recent experimentation has shown that the specific heat of carbon nanotubes increases linearly with temperature from 2 K to 8 K, with an increase in the slope above 8 K.[26] This behavior implies a quantized 1D phonon spectrum in carbon nanotubes at temperatures below 8 K. Above 8 K, the number of phonon modes excited becomes large enough to make the specific heat appear to be continuous with temperature. Therefore, quantum thermal effects are not seen at the temperatures used in these simulations. Furthermore, the use of Fourier's classical law of heat flow in the MD simulations precludes the inclusion of quantum thermal effects. Fourier's law provides an aggregate measure of the thermal conductivity by summing over all of the present phonon modes,[39] but in doing so wipes out information about the contribution of individual phonons to heat flow. It has been demonstrated that the thermal conduction of carbon nanotubes at any temperature is dominated by phonons.[19] Therefore, it is possible that a more detailed model including a consideration of individual phonon modes may reveal thermal rectification in Y-junction nanotubes at very low temperatures.

The discontinuity in the temperature profile of the Y-junction nanotube seems to be the result of the discontinuous crystal structure present at the hub of the Y-junction. Similar temperature profiles have been observed in crystal grain boundaries,[37] junctions between nanotubes of different diameters,[38] and in single nanotubes with vacancy defects present. A study of the phonon modes in the investigated tubes indicates that the presence of defects reduces the density of axial and radial phonon modes. This connection between the temperature discontinuity and the atomic vibrations seems to indicate that both the axial and the radial modes are at least partly responsible for the transfer of heat along a nanotube, and that the interruption of these modes results in an interruption of heat transfer.

CHAPTER FIVE

HEAT PULSE PROPAGATION

5.1. Introduction

In Chapter 4, the details of the simulation of steady state heat flow through a Y-junction carbon nanotube were provided. In this chapter, the transient heat flow properties of the Y-junction nanotube are examined. Molecular dynamics simulations are used to generate a heat pulse in the Y-junction and examine how it propagates through the structure. In this chapter, the simulation method is described, the results are summarized and an analysis is provided.

5.2. Methodology

The details of the molecular dynamics simulation used in the study of heat pulse propagation are similar to those presented in Chapter 4. As before, the Tersoff-Brenner bond order potential has been used. The general simulation method, as described in Chapter 3, is exactly the same. The difference lies in the application of heat to the system. In the steady state case, hot and cold thermal reservoirs were placed at opposite ends of the Y-junction to induce heat flow. The temperatures of these reservoirs were maintained by velocity scaling through equation (4.1). In the case of transient heat flow, the setup is slightly different, and can be seen in figure 5.1.

The slabs labeled “Fixed” and those labeled “Buffer” are the same as those described in Chapter 4. The buffer slabs are maintained at the ambient temperature of the simulation. The slabs labeled “Pulse” are those to which the heat pulse is applied. The temperature in the “Pulse”

slabs is controlled through velocity scaling as in equation (4.1), but instead of being constant, $T_{control}$ is time-dependent. This time-dependence can be seen in figure 5.2.

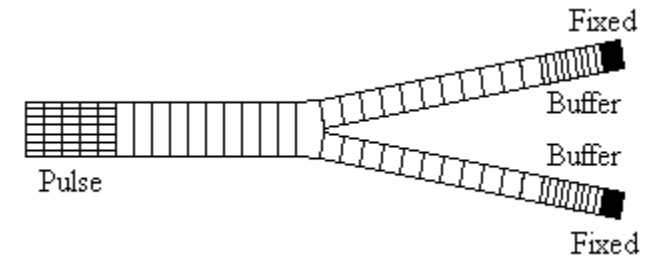

Figure 5.1: Molecular dynamics setup for applying a heat pulse to the Y-junction carbon nanotube.

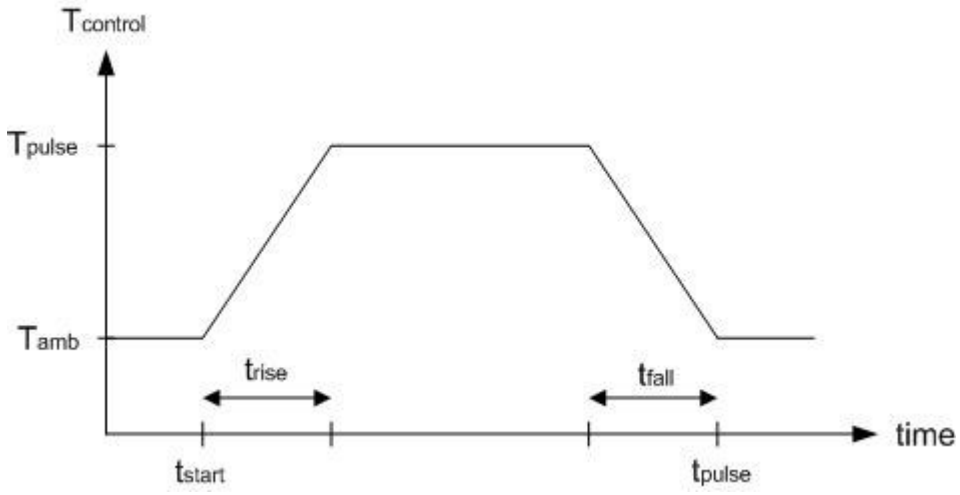

Figure 5.2: Time-dependent behavior of the applied heat pulse.

From this figure it should be noted that T_{amb} is the same ambient temperature at which the buffer slabs are held. Before and after the heat pulse, the temperature of the "Pulse" slabs is maintained at T_{amb} in the same manner as the buffer slabs, with one small adjustment. There is no fixed slab at the end of the tube where the pulse is applied. This is done in order to minimize

reflections from that tube end. However, the absence of a fixed slab results in the possibility of large-scale oscillations on that end of the tube. These oscillations would be greatly magnified by velocity scaling during the application of the heat pulse. Therefore, at each time step the center-of-mass velocity of the pulse slabs is calculated and subtracted from the velocity of each atom. This ensures that the overall momentum of this end of the tube remains zero.

Because this simulation is a transient one, there is no need to calculate properties based on statistical averages, such as thermal conductivity or the velocity autocorrelation function. Instead, it is only necessary to collect the temperature profile data at specific time intervals throughout the simulation. This data provides the time evolution of the temperature at each point in the Y-junction nanotube. However, the instantaneous temperature data can be noisy in both time and space. Therefore, two techniques, spatial and temporal averaging, are used to provide a smoother picture of the time evolution of the temperature. Spatial averaging determines the local temperature of each slab by finding the average temperature of the current slab and its two nearest neighbor slabs on each side. For example, the local temperature of slab 10 is the average temperature of slabs 8, 9, 10, 11, and 12. In temporal averaging, the temperature of a slab at the current time step is equal to the average of the temperature of that slab over the previous N time steps.

5.3. Results

The Y-junction used in these simulations had a (14,0) trunk and two (7,0) branches. Each branch contained 150 slabs, for a total of 451 slabs and 16,860 atoms. With a slab-width of 4.26 Å, each branch measured about 64 nm long. This is long enough to examine the propagation of heat pulses through the branches before they reach the junction. The Y-junction nanotube was

simulated under three different heat pulse configurations: a heat pulse originating in the (14,0) trunk, a heat pulse originating in one of the (7,0) branches, and a heat pulse originating in both of the (7,0) branches simultaneously. Each simulation was run for 30,000 time steps. At 0.5 fs per step, this is a total time of 15 ps. For comparison, a straight (14,0) nanotube and a straight (7,0) nanotube each measuring 300 slabs (128 nm) were also run under the heat pulse simulations. Temporal averaging was taken over an interval of 50 time steps. In each case, the tube in question was quenched to $T_{amb} = 0$ K, while the pulse magnitude was $T_{pulse} = 800$ K. The rise and fall times were $t_{rise} = t_{fall} = 100$ steps (50 fs), the start time was $t_{start} = 1$ time step, and the pulse length was $t_{pulse} = 2000$ time steps (1 ps).

Figure 5.3 shows the results of the heat pulse simulation on the (7,0) carbon nanotube. As seen in this figure, the heat pulse has excited several traveling waves. Three of them are of particular interest in this discussion, and are labeled in figure 5.3. The wave labeled "1" is the leading edge wave, and travels at a speed of 21.3 km/sec. This speed is consistent with the sound velocity of longitudinal acoustic phonons in (10,10) armchair nanotubes, which are estimated to be 20.35 km/sec, and that of 21.0 km/sec in 3D graphite.[40] The magnitude of this leading wave is very small, on the order of 3 K. The second wave of interest, labeled "2," travels at approximately 12.8 km/sec, which is similar to the sound velocity of the transverse acoustic mode in 3D graphite at 12.3 km/sec. The velocities of the transverse acoustic mode of a (10,10) nanotube and 2D graphite are estimated to be 9.4 km/sec and 15.0 km/sec, respectively, and the velocity of the twisting mode of a (10,10) nanotube is approximately 15.0 km/sec.[40] The magnitude of this wave is relatively large, on the order of 130 K. The final mode of interest, labeled "3," travels at 6.4 km/sec and precedes diffusive heat flow in the (7,0) nanotube, due to increase in overall temperature behind it. The leading wave in the diffusive heat flow has a

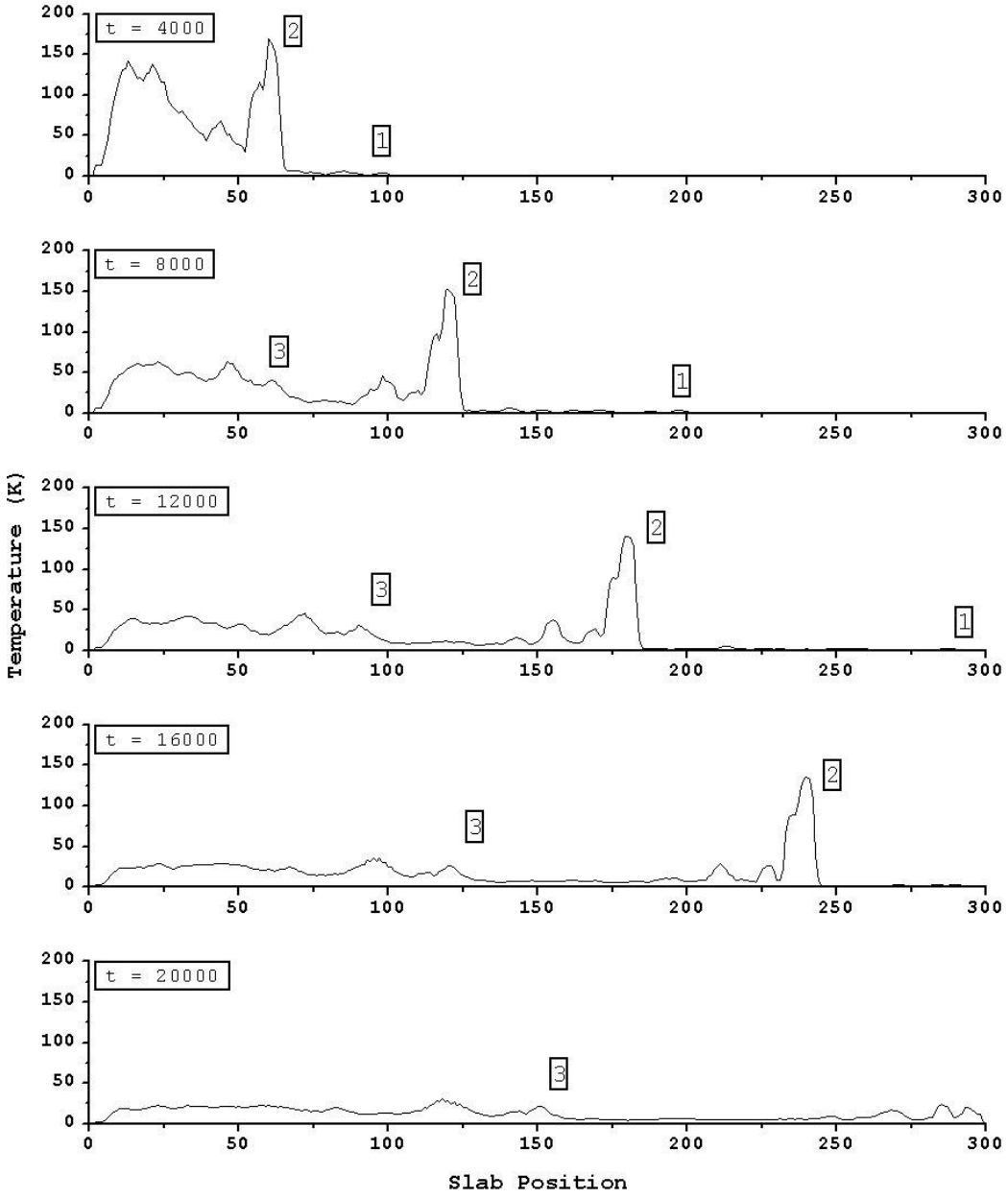

Figure 5.3: Heat pulse results of the (7,0) carbon nanotube.

magnitude on the order of 25 K. Henceforth, these waves will be known as type-1, type-2 and type-3 waves, corresponding to their labels in figure 5.3. The waves seen in subsequent figures will also be labeled accordingly.

Figure 5.4 shows the results of the heat pulse simulation on the (14,0) carbon nanotube. The labeled waves correspond to those in figure 5.3. The type-1 leading edge wave of the (14,0) nanotube travels at a velocity of 18.3 km/sec, and has a magnitude on the order of 0.5 K. The type-2 wave travels at approximately 12.1 km/sec, with a magnitude of about 70 K. The type-3 wave travels at 5.5 km/sec with a maximum pulse magnitude of around 50 K. From these results it can be seen that these waves propagate slightly slower in the (14,0) nanotube than they do in the (7,0) nanotube. One other thing to note is that the type-2 wave appears to have a second peak trailing along behind it at the same velocity. This could be the result of a reflection of this wave off the tube end, which would explain its reduced magnitude. It is unclear why this is not observed in the (7,0) nanotube.

Figure 5.5 shows the results when the heat pulse is applied to both branches simultaneously. In this figure, slabs 1-150 represent the (14,0) trunk region. The solid curve along slabs 152-301 represents the first (7,0) branch, while the broken curve represents the second one. Slab 151 is the hub of the Y-junction structure. The vertical broken line at slab 150 is used to indicate the location of the junction. In this figure, it can be seen that some of the waves that reach the junction are transmitted into the (14,0) trunk, but with a reduced magnitude. The waves of interest in this figure have been labeled corresponding to their type. At t = 5000 time steps, one can see that type-1 and type-2 waves are propagating in the branches toward the junction at about 19.0 km/sec and 10.6 km/sec, respectively. It appears that the magnitude of the type-2 wave in branch 2 is larger than that in branch 1. This could be due to a variation in the initial noise conditions of the branches. The tube was quenched at a low temperature for a long time, but perhaps only a slight difference in noise conditions can result in a magnitude difference of this scale.

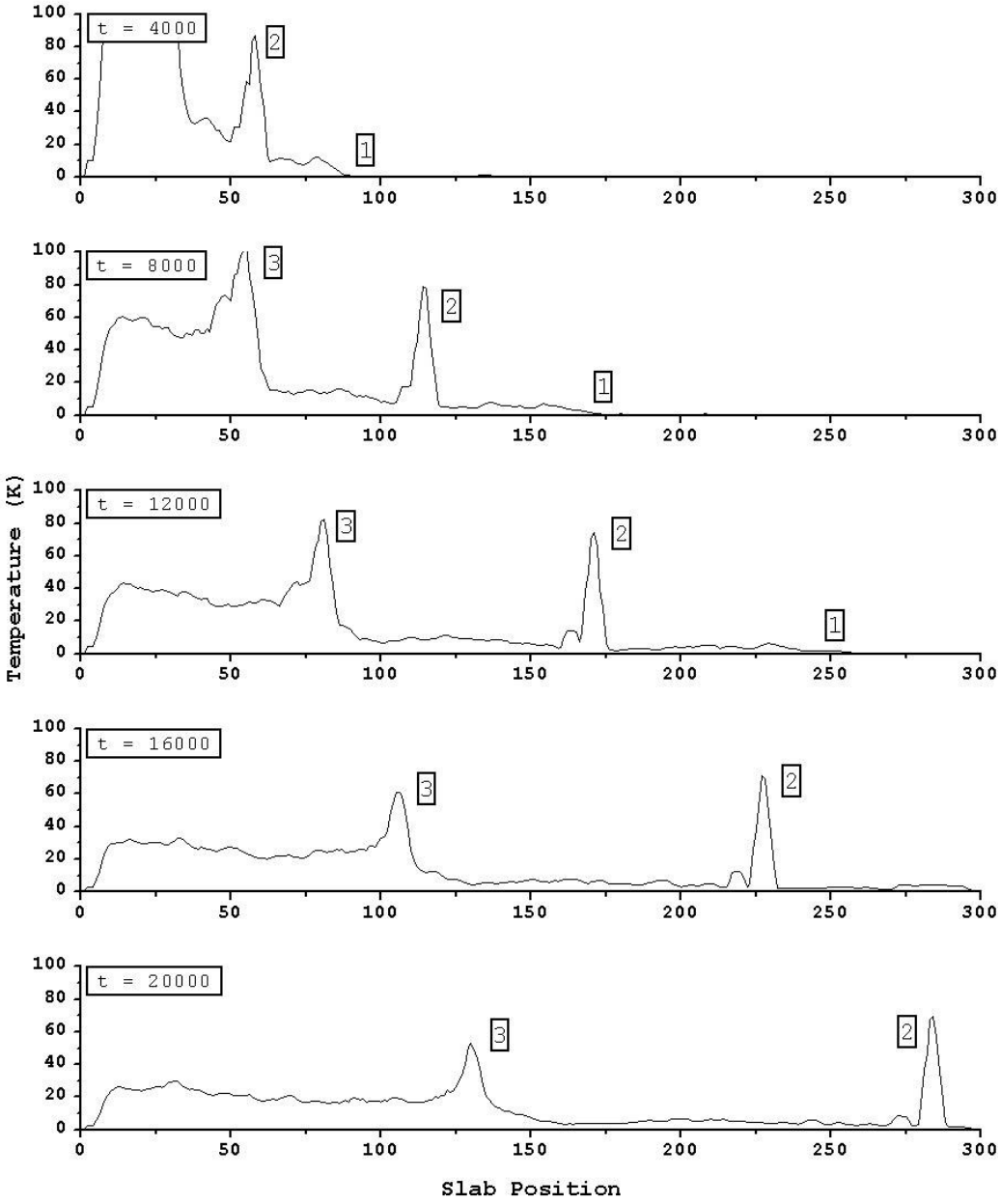

Figure 5.4: Heat pulse results of the (14,0) carbon nanotube.

At t = 10000 time steps, the type-1 wave has passed into the trunk, still traveling at about 19.0 km/sec, while the type-2 wave is very near the junction. One can also see the appearance of the type-3 wave, traveling at about 6.8 km/sec. At t = 13000 time steps, one can see that the

type-2 waves in the branches have collided with the junction, and have partially reflected back into the branches. As a result, two waves have been generated in the trunk, one traveling at a velocity of 9.5 km/sec and the other traveling at a velocity of 6.4 km/sec. These waves have been labeled "2a" and "2b," respectively. At t = 18000 time steps, these two waves continue to propagate in the trunk, and the type-3 waves in the branches approach the junction. At t = 25000 time steps, one can see that the type-3 waves in the branches have passed through the junction into the trunk, continuing to travel at 6.4 km/sec. It appears that the magnitude of diffusive heat flow has been significantly reduced upon passing into the trunk.

In figure 5.6, the heat pulse has been applied to only one of the branches. The behavior observed in figure 5.5 is essentially the same as that seen here, except for the fact that the magnitudes of the waves that propagate into the trunk are much smaller. It is also possible to see that the type-2 wave from branch 1 has propagated into branch 2.

Figure 5.7 shows the results when the heat pulse is applied to the (14,0) trunk. At t = 5000 time steps the type-1 leading wave is evident, traveling at about 19.0 km/sec. At t = 10000, the type-2 and type-3 waves become discernable, traveling at 11.4 km/sec and 5.8 km/sec, respectively. At this time, the type-1 wave has passed into the branches and maintained its velocity. At t = 13000, the type-2 wave has partially reflected back into the trunk, and has transmitted three waves into the branches. These are labeled "2a," "2b," and "2c" and travel at 10.4 km/sec, 8.4 km/sec and 6.3 km/sec, respectively. At t = 18000, the type-3 wave has propagated closer to the junction, maintaining its speed. At t = 25000, the type-3 wave has partially reflected back into the trunk. The portion of the wave transmitted to the trunk has split into several waves, all traveling around 5.8 km/sec. However, it is difficult to distinguish them because waves 2a-2c have reflected off the ends of the branches, causing interference. As in

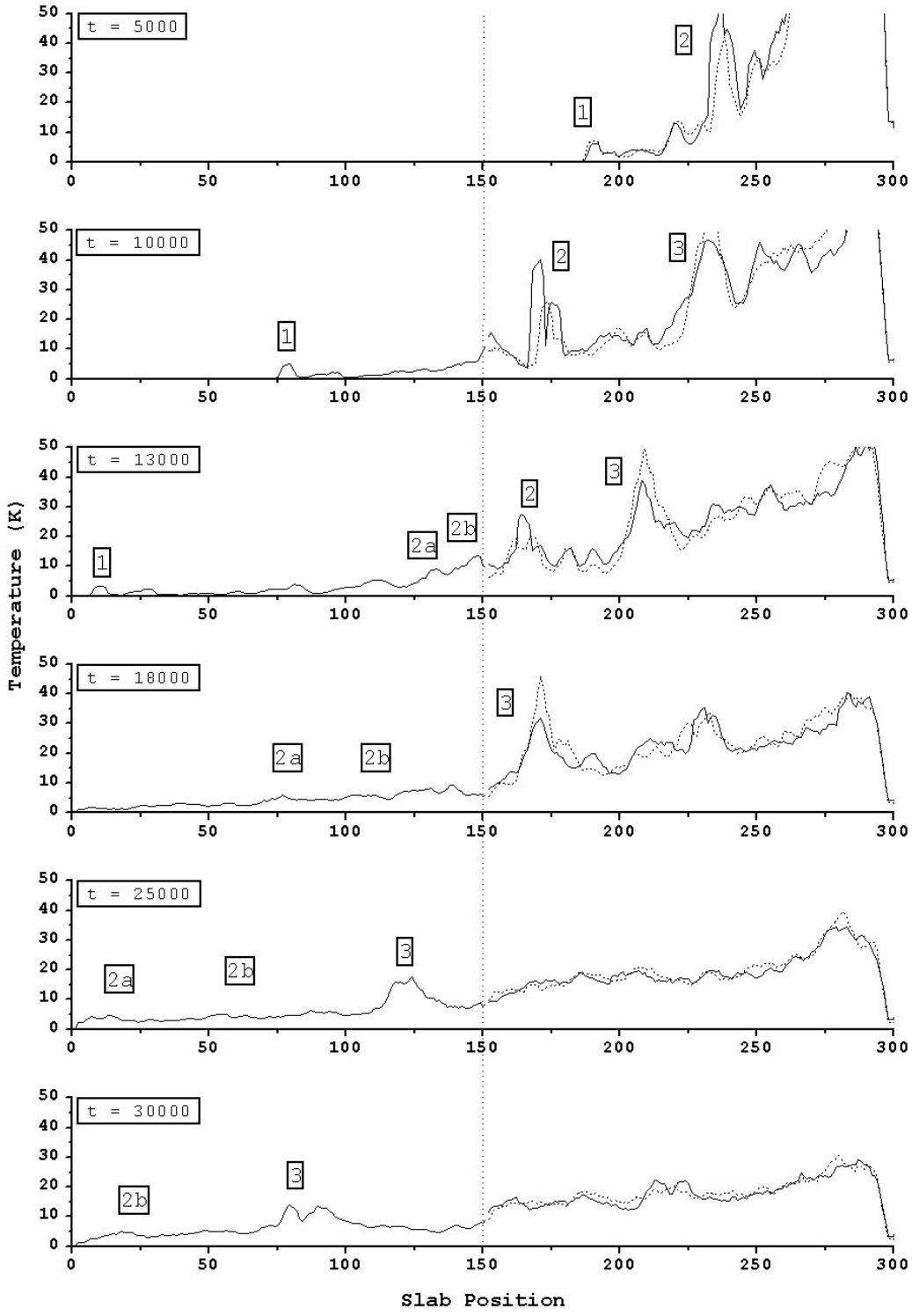

Figure 5.5: Heat pulse results of the Y-junction carbon nanotube with the pulse applied to both branches simultaneously.

figure 5.5, it appears that the diffusive heat flow has been significantly reduced upon passing through the junction.

5.4. Discussion

The results in figures 5.3 and 5.4 indicate that a heat pulse can excite many traveling waves in straight carbon nanotubes. The leading edge waves in both the (7,0) and (14,0) tubes travel at a speed that corresponds to the speed of longitudinal acoustic waves in other carbon nanotubes and in graphite. This suggests that the type-1 leading edge wave in figures 5.3 and 5.4 is also a longitudinal mode. Several other waves trail along behind this, including a relatively large one that travels at 12-13 km/sec in each nanotube. This may correspond to either a transverse mode or a twisting mode. Diffusive heat flow came along more slowly, at 6.7 km/sec in the (7,0) nanotube and 5.5 km/sec in the (14,0) nanotube.

In Chapter 4, it was found that the thermal conductivity of the Y-junction carbon nanotube did not appear to be dependent on the direction of heat flow at temperatures around room temperature. However, in the case of heat pulse propagation at very low temperatures, some asymmetry does appear. From figures 5.5 and 5.7, it appears that individual traveling waves can pass through the junction in either direction. However, these results show that thermal energy in the form of traveling waves appears to transmit through the junction better when passing from the trunk to the branches than it does in the opposite direction.

By comparing figures 5.5 and 5.6, it is evident that traveling waves are best transferred from the branches to the trunk if they arrive from both branches simultaneously, or in phase. Thus, it can be assumed that atomic vibrations that reach the junction out of phase will not give rise to modes that can propagate into the trunk. This can explain why traveling waves are not

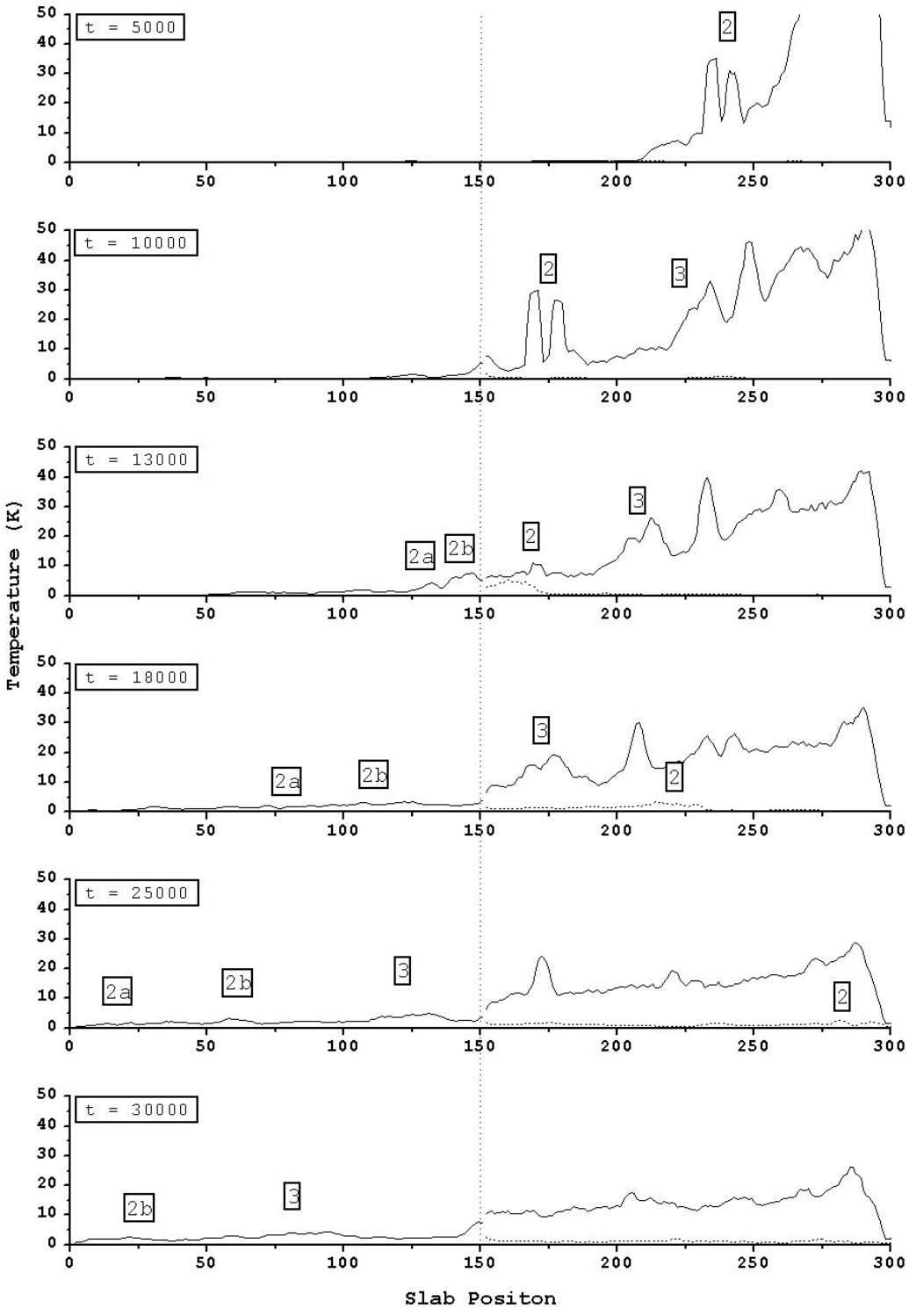

Figure 5.6: Heat pulse results of the Y-junction carbon nanotube with the pulse applied to one branch.

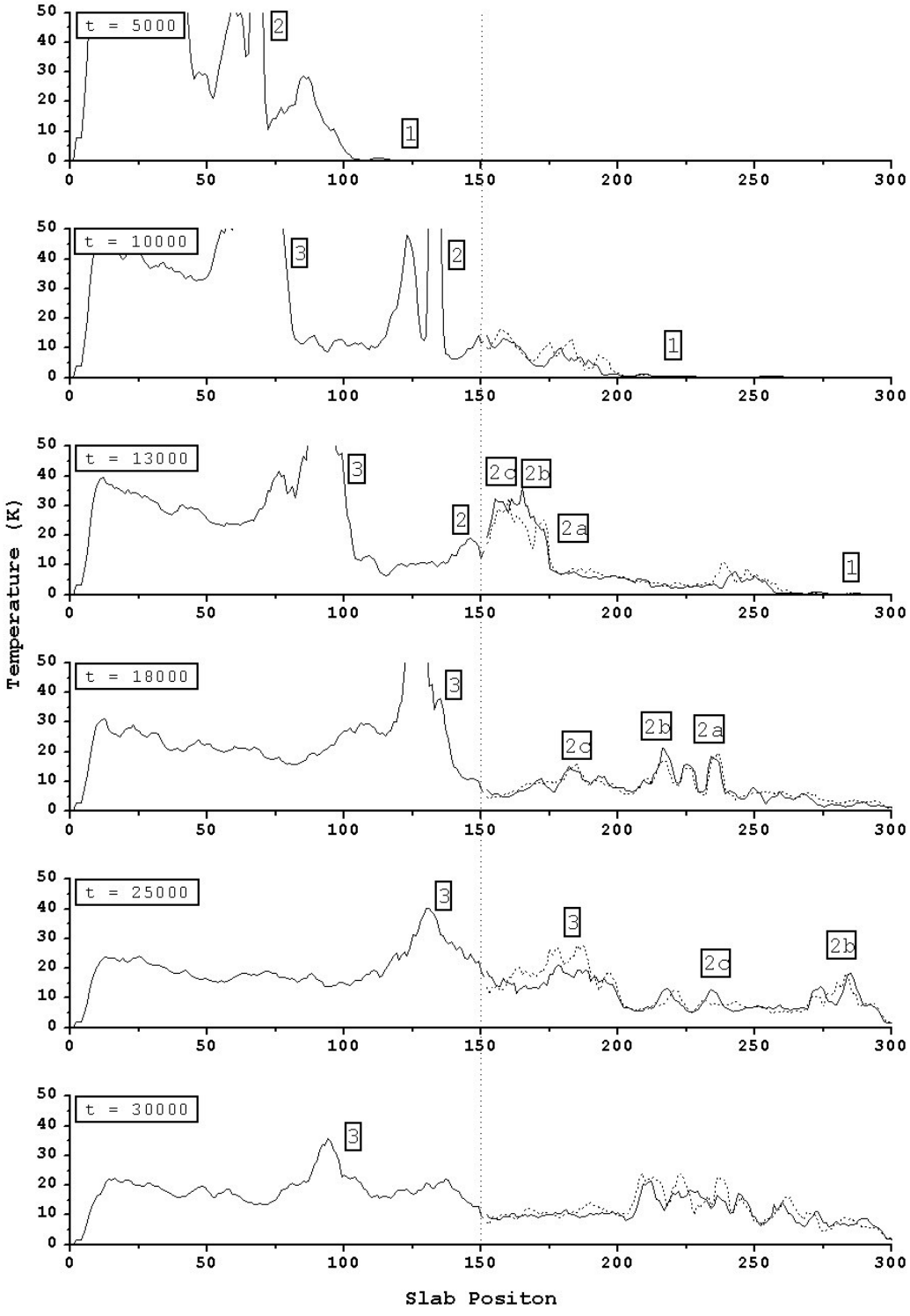

Figure 5.7: Heat pulse results of the Y-junction carbon nanotube with the pulse applied to the trunk.

transferred very well into the trunk from the branches. Each wave is made up of a distribution of atomic vibrations. Although two waves may reach the junction at the same time, it is not expected that the vibrations associated with these waves will be in phase with one another, and thus interference will occur, blocking heat from flowing from the branches to the trunk. When heat is passing from the trunk to the branches, the phase nature of the atomic vibrations is not important because the trunk is the only source of heat. Thus, the traveling waves pass more easily from the trunk into the branches.

In figures 5.5-5.7 it was seen that traveling waves could split into several new waves upon passing through the junction. Each of these new waves traveled at a velocity less than or equal to the original wave. This suggests that traveling waves can act as a heat source at the junction, but that their inherent energy content limits which new waves can be generated. It is also possible that a traveling wave's orientation will determine which waves are generated when it hits the junction. Extra molecular dynamics code would have to be written to determine whether a traveling wave consists of longitudinal vibrations, transverse vibrations, or some combination of the two.

In figure 5.5 it was seen that the magnitudes of the type-2 waves in the branches are significantly different. Furthermore, their magnitudes are much smaller than the magnitude of the type-2 wave seen in the straight (7,0) nanotube in figure 5.3. Figure 5.7 indicates that traveling waves are transmitted very well from the trunk to the branches. However, an earlier simulation showed that this was not the case; the traveling waves in the trunk had mostly died out by the time they reached the junction. The newer simulation was used in this case because the Y-junction nanotube was quenched to 0 K for a longer period of time; there was still some thermal noise in the prior simulation. Other simulations of the straight (14,0) nanotube have

resulted in a type-2 wave that was nearly nonexistent. Figures 5.5 and 5.7 seem to indicate that traveling waves pass through the junction better when they originate in the trunk. However, this may only appear to be the case because the magnitudes of the waves that reach the junction in figure 5.7 are much greater than those in figure 5.5.

There appears to be a good deal of inconsistency in the magnitude and stability of the waves that are generated by the heat pulse. The cause of these issues seems to lie with the initial state of the carbon nanotube being simulated. Before a heat pulse is applied, the nanotube is quenched to a temperature negligibly above 0 K. This quenching is done with the application of friction and random forces, as is done with the buffer slabs in figure 4.2. It has been observed that a carbon nanotube quenched for a certain number of time steps will have a different heat pulse response than the same nanotube quenched for a different number of time steps. Because these nanotubes have been quenched for a different number of time steps, the velocities of the atoms in the pulse slabs will most likely have different random distributions. When velocity scaling is applied to generate the heat pulse, these velocities will be scaled to very large values. So, while the differences in initial conditions may not matter at low temperatures, they appear to matter when the pulse is applied.

CHAPTER SIX

CONCLUSION

Molecular dynamics simulations have been used to examine the thermal properties of a Y-junction carbon nanotube under steady state and transient conditions. The steady state simulations have revealed that the thermal conductivity of a Y-junction carbon nanotube is less than that of a corresponding straight nanotube. This drop in thermal conductivity is the result of the interruption of lattice continuity at the junction. The junction acts to impede heat flow by suppressing the density of phonon modes in the system. This manifests itself in the form of a discontinuity in the temperature profile of the Y-junction nanotube. Furthermore, it has been found that the thermal conductivity is independent of the direction of heat flow. This is in contrast to results obtained for electrical current flow. The calculations involving electrical rectification included the effects of quantum electronic states. At room temperature, enough phonon modes have been excited that the thermal properties of carbon nanotubes appear to be continuous in nature. Furthermore, the method of simulation used in this research is entirely classical, and does not account for the contribution of individual phonon modes. However, experiments have indicated the existence of quantized thermal conductance at very low temperatures. Therefore, a method of simulation that accounts for quantum thermal effects may reveal thermal rectification at low temperatures.

The heat pulse simulations have revealed that some asymmetry in heat flow appears to occur. Traveling waves were shown to pass fairly well from the trunk to the branches, but not so well in the opposite direction. This was attributed to atomic vibrations of a wave in one branch being out of phase with those in the other branch when they reached the junction. Diffusive heat flow appeared to be limited in both directions. It was also seen that it is possible for a wave to

split into several waves when passing through the junction. The velocities of the new waves were always less than or equal to the velocities of the original wave. Finally, it was noted that there were significant inconsistencies in the magnitude and stability of the waves generated by the heat pulse. These were attributed to variations in the initial state of the carbon nanotube that get blown up when the heat pulse is applied.

There are several possibilities for future work. First, the steady state simulations could be adapted to determine if thermal rectification does occur at very low temperatures. These simulations will have to account for the individual contribution of phonons to heat flow. For the heat pulse simulations, extra code could be added to determine the orientation of the various modes that propagate through the nanotubes. In addition, the issue of initial conditions in the nanotubes needs to be addressed. Finally, all of these simulations can be run again using other Y-junction nanotubes.

REFERENCES

[1] G. D. Hutcheson, "The First Nanochips," Scientific American **290**, Issue 4, 76 (2004).

[2] S. Iijima, "Helical microtubules of graphitic carbon," Nature **354**, 56 (1991).

[3] R. Saito, M. Fujita, G. Dresselhaus and M.S. Dresselhaus, "Electronic structure of graphene tubules based on C_{60}," Physical Review B **46**, 1804 (1992).

[4] N. Hamada, S. Sawada and A. Oshiyama, "New One-Dimensional Conductors: Graphitic Microtubules," Physical Review Letters **68**, 1579 (1992).

[5] S. Berber, Y. Kwon and D. Tománek, "Unusually High Thermal Conductivity of Carbon Nanotubes," Physical Review Letters **84**, 4613 (1996).

[6] M. Menon and D. Srivastava, "Carbon Nanotube 'T Junctions': Nanoscale Metal-Semiconductor-Metal Contact Devices," Phys. Rev. Lett. **79**, 4453 (1997).

[7] M. Menon and D. Srivastava, "Carbon nanotube based molecular electronic devices," J. Mat. Res. **13**, 2357 (1998).

[8] M. Terrones, F. Banhart, N. Grobert, J.-C Charlier, H. Terrones, and P. M. Ajayan, "Molecular Junctions by Joining Single-Walled Carbon Nanotubes," Phys. Rev. Lett. **89**, 75505 (2002).

[9] L. Jing, C. Papadopolous, and J. Xu, "Growing Y-junction carbon nanotubes," Nature **402**, 253 (1999).

[10] A. Andriotis, M. Menon, D. Srivstava and L. Chernozatonskii, "Transport properties of single-wall carbon nanotube Y junctions," Physical Review B **65**, 165416 (2002).

[11] C. Papadopoulos, A. Rakitin, J. Li, A.S. Vedeneev and J.M. Xu, "Electronic Transport in Y-Junction Carbon Nanotubes," Physical Review Letters **85**, 3476 (2000).

[12] R. Saito, G. Dresselhaus and M.S. Dresselhaus, Physical Properties of Carbon Nanotubes, Imperial College Press, London (1998).

[13] V. Crespi, "Relations between global and local topology in multiple nanotube junctions," Physical Review B **58**, 12671 (1998).

[14] R. Saito, M. Fujita, G. Dresselhaus and M.S. Dresselhaus, "Electronic structure of chiral graphene tubules," Applied Physics Letters **60**, 2204 (1992).

[15] T.W. Odom, J. Huang, P. Kim and C.M. Lieber, "Atomic structure and electronic properties of single-walled carbon nanotubes," Nature **391**, 62 (1998).

[16] L. Chico, V.H. Crespi, L.X. Benedict, S.G. Louie and M.L. Cohen, "Pure Carbon Nanoscale Devices: Nanotube Heterojunctions," Physical Review Letters **76**, 971 (1996).

[17] Z. Yao, H.W. Postma, L. Balents and C. Dekker, "Carbon nanotube intramolecular junctions," Nature **402**, 273 (1999).

[18] C. Kittel, Introduction to Solid State Physics, John Wiley and Sons, New York (1996).

[19] J. Hone, M. Whitney, C. Piskoti and A. Zettl, "Thermal conductivity of single-walled carbon nanotubes," Physical Review B **59**, 2514 (1999).

[20] M.A. Osman and D. Srivastava, "Temperature dependence of the thermal conductivity of single-wall carbon nanotubes," Nanotechnology **12**, 21 (2001).

[21] J. Che, T. Cagin and W.A. Goddard III, "Thermal conductivity of carbon nanotubes," Nanotechnology **11**, 65 (2000).

[22] J. Hone, M.C. Llaguno, N.M. Nemes and A.T. Johnson, "Electrical and thermal transport properties of magnetically aligned single wall carbon nanotube films," Applied Physics Letters **77**, 666 (2000).

[23] P. Kim, L. Shi, A. Majumdar and P.L. McEuen, "Thermal Transport Measurements of Individual Multiwalled Nanotubes," Physical Review Letters **87**, 215502 (2001).

[24] L.G.C. Rego and G. Kirczenow, "Quantized Thermal Conductance of Dielectric Quantum Wires," Physical Review Letters **81**, 232 (1998).

[25] K. Schwab, E.A. Henrikson, J.M. Worlock and M.L. Roukes, "Measurement of the quantum of thermal conductance," Nature **404**, 974 (2000).

[26] J. Hone, B. Batlogg, Z. Benes, A.T. Johnson and J.E. Fischer, "Quantized Phonon Spectrum of Single-Wall Carbon Nanotubes," Science **289**, 1730 (2000).

[27] D.C. Rapaport, The Art of Molecular Dynamics Simulation, Cambridge University Press, Cambridge (1995).

[28] M.P. Allen and D.J. Tildesley, Computer Simulation of Liquids, Clarenden Press, Oxford (1987).

[29] J. Tersoff, "New empirical approach for the structure and energy of covalent systems," Physical Review B **37**, 6991 (1988).

[30] J. Tersoff, "Empirical Interatomic Potential for Carbon, with Applications to Amorphous Carbon," Physical Review Letters **61**, 2879 (1988).

[31] D.W. Brenner, "Empirical potential for hydrocarbons for use in simulating the chemical vapor deposition of diamond films," Physical Review B **42**, 9458 (1990).

[32] C. Kittel and H. Kroemer, Thermal Physics, W.H. Freeman and Company, New York (1980).

[33] D.A. McQuarrie, Statistical Mechanics, Harper and Row, New York (1976).

[34] C. Oligschleger and J.C. Schön, "Simulation of thermal conductivity and heat transport in solids," Physical Review B **59**, 4125 (1999).

[35] F. Müller-Plathe, "A simple nonequilibrim molecular dynamics method for calculating thermal conductivity," Journal of Chemical Physics **106**, 6082 (1997).

[36] D.J. Evans and G.P. Morriss, Statistical Mechanics of Nonequilibrium Liquids, Academic Press, London (1990).

[37] A. Maiti, G. Mahan, and S. Pantelides, "Dynamical simulations of nonequilibrium processes – heat flow and the Kapitza resistance across grain boundaries," Solid State Communications **102**, 517 (1997).

[38] S. Maruyama, Y. Taniguchi, and Y. Shibuta, "Characterization of Heat Conduction of Carbon Nanotube by Molecular Dynamics Method," Eurotherm 75, Champagne (2003).

[39] R. Berman, Thermal Conduction in Solids, Clarendon Press, Oxford (1976).

[40] R. Saito, T. Takeya, T. Kimura, G. Dresselhaus and M.S. Dresselhaus, "Raman intensity of single-wall carbon nanotubes," Physical Review B **57**, 4145 (1998).